

Towards numerical two-loop integrand reduction

Giuseppe Bevilacqua,^a Dhimiter Canko,^b Costas Papadopoulos,^a Aris Spourdalakis^{a,c,d}

^a*Institute of Nuclear and Particle Physics, NCSR Demokritos, Patr. Grigoriou E' & 27 Neapoleos Str, 15341 Agia Paraskevi, Greece*

^b*Dipartimento di Fisica e Astronomia, Università di Bologna e INFN, Sezione di Bologna, Via Irnerio 46, I-40126 Bologna, Italy*

^c*University of Debrecen, Faculty of Science and Technology, Department of Experimental Physics, 4010, Debrecen, PO Box 105, Hungary*

^d*Institute for Theoretical Physics, ELTE Eötvös Loránd University, Pázmány Péter sétány 1/A, H-1117 Budapest, Hungary*

ABSTRACT: We present a method for the integrand-level reduction of two-loop helicity amplitudes in both $d = 4 - 2\epsilon$ and $d = 4$ dimensions. The amplitude is expressed in terms of a set of Feynman integrals and their coefficients that depend on the external kinematics. The analysis presented in this paper, in conjunction with the ongoing development of the computational framework **HELAC-2LOOP**, paves the road for the construction of an automated program for two-loop amplitude calculations for arbitrary scattering processes.

KEYWORDS: Scattering Amplitudes, QCD Phenomenology, NNLO Computations, Integrand reduction

Contents

1	Introduction	1
2	Description of the method	3
2.1	Basic notation and conventions	3
2.2	Linear fit and fit by cut approach	5
2.3	Global fit approach	7
2.4	Projecting over a full family	8
3	Application of the method	10
3.1	Four-Point Kinematics	11
3.1.1	Double-box topologies	11
3.1.2	Penta-triangle topologies	16
3.1.3	Hexa-bubble topologies	18
3.1.4	Non-planar double box topologies	19
3.1.5	$gg \rightarrow t\bar{t}$	21
3.2	Five-Point Kinematics	23
3.2.1	Penta-box topologies	23
3.2.2	$t\bar{t}H$	25
3.3	Six-Point Kinematics	27
3.3.1	Six-gluon topology	27
4	Summary and Discussion	28

1 Introduction

Several decades after its establishment, the Standard Model (SM) keeps offering a successful description of Strong and Electroweak interactions among fundamental particles. One of the most concrete and reliable ways of probing the SM is the comparison of its predictions to experimental data from high-energy particle collisions. The present energy frontier is represented by the Large Hadron Collider (LHC) with its four experiments, CMS, ATLAS, ALICE, and LHCb. The forthcoming High Luminosity upgrade of the LHC (HL-LHC) will significantly boost the statistical accuracy of the experimental data that are being collected, allowing experiments to reach percent-level precision in many cases [1–3]. The accurate interpretation of the data from the LHC, as well as from possible future colliders [4], demands theoretical predictions of comparable precision.

Theoretical predictions are formulated from first principles within the framework of perturbative Quantum Field Theory, where scattering cross sections and other observables are computed as a power series expansion in the coupling constants of the SM. The first

term in this expansion corresponds to the leading-order (LO) contribution, followed by subsequent corrections at next-to-leading order (NLO), next-to-next-to-leading order (NNLO), and so on. The calculation of NNLO corrections (and occasionally even N³LO) is necessary in order to meet the current (and near future) experimental precision. The bottleneck for most NNLO calculations consists, at present, of the computation of double-virtual corrections, which rely upon two-loop dimensionally regularized scattering amplitudes. As the number of particles in a process increases, the complexity of the latter increases dramatically. The current frontier is the calculation of $2 \rightarrow 3$ processes [5], with several results in this direction being achieved in recent years [6–34] as the product of considerable effort from the theoretical community.

The calculation of two-loop amplitudes can be regarded as a three-step procedure. The initial step involves the construction of the amplitude through the use of standard Feynman graph generation [35, 36] or recursive approaches [37, 38]. The second step includes the reduction of the amplitude into a set of independent Feynman integrals, commonly known as *master integrals*. For this to be achieved, the constructed amplitude should be projected into a set of scalar Feynman integrals, which can be done using tensor [39–43], or integrand [44–56] reduction methods. The generated scalar integrals from these methods need to be furthermore reduced, at the integral level, into master integrals using *integration-by-parts* (IBP) identities [57–59], satisfied by the Feynman integrals within dimensional regularization ($d = 4 - 2\epsilon$). The latter field has benefited from the application of *finite-field techniques* [60, 61] for solving IBP identities, and the recent advancements in the generation of optimized IBP systems, utilizing *syzygy equations* [62, 63] and the *block-triangular form* [64, 65]. The last step for the computation of the scattering amplitude is the evaluation of the master integrals resulting from the reduction, which can be attained by methods such as *sector decomposition* [66–68], *differential equations* [69–74], *auxiliary mass flow* [75, 76], and *dimension-changing transformation* [77, 78].

The present work focuses on the second step of the aforementioned procedure, and more specifically on the integrand reduction of two-loop scattering amplitudes into scalar integrals. In the one-loop case, the integrand reduction *OPP method* [79], demonstrated a systematic algebraic approach to the computation of amplitudes, based upon solving *cut equations*, meaning equations resulting from setting some (or all) of the inverse propagators to zero, following a top-down approach. Integrand reduction has been implemented in various numerical algorithms [80–92] and has boosted automation of NLO computations. Our goal is to extend the OPP method to two-loop calculations [44–54]. We investigate two-loop amplitude reduction at the integrand level, in $d = 4 - 2\epsilon$ and $d = 4$ dimensions, by solving cut equations in a top-down approach [44–47, 52–54, 56] in several two-loop examples. In general, to facilitate computations, Feynman integrals that share the same topological and kinematical structure can be grouped into *integral families*. A novel element of our study is the extension of the cut equations to include all inverse propagators characterizing a provided integral family and not just the ones of the Feynman graph under consideration. This approach yields a larger number of systems of equations to be solved, albeit smaller in size, and has the advantage of allowing the reduction of all the Feynman graphs that belong to the same family altogether. Furthermore, we study an alternative method for

integrand-level reduction that does not rely on cut equations, but rather on sampling the integrand's numerator over random values of loop momenta.

This paper is structured as follows. In section 2, the notation employed is introduced, and the general ideas and concepts of the methods studied are explained. In section 3, the application of these methods to several examples with different kinematics is presented, ranging from four- to six-particle processes. In section 4, we conclude by giving a summary of our study and its prospects for the future.

2 Description of the method

2.1 Basic notation and conventions

A generic unrenormalized L -loop scattering amplitude can be written schematically as

$$\mathcal{A}^{(L)}(\{p\}) = \sum_{g=1}^G \left(\int \prod_{i=1}^L [dk_i] \frac{\mathcal{N}(k_1, \dots, k_L, \{p\})}{D_1 D_2 \dots D_n} \right)_g, \quad (2.1)$$

where k_1, \dots, k_L are loop momenta, $[dk_i]$ denotes the integration measure associated to the loop momentum k_i , and $\{p\}$ represents the set of external kinematics. The amplitude consists generally of G partial contributions, individually denoted by g . Depending on the considered approach, the latter may be individual Feynman diagrams or consistently defined sub-amplitudes. In the following, we will refer to them as *loop topologies*. In what follows, we focus on the genuine two-loop contributions to the amplitude (so-called Theta topologies), namely those that cannot be trivially reduced to the product of one-loop ones (Infinity and Dumbbell topologies)¹. Each loop topology is characterized by a *numerator* \mathcal{N} , which is a function of external momenta and wavefunctions as well as loop momenta, and by a product of n *inverse propagators* D_1, \dots, D_n , appearing in its denominator².

The first step towards constructing a reduction method for two-loop calculations is to parametrize the numerator \mathcal{N} in terms of the inverse propagators, moving along the path set by Ref. [79]. A few comments are in order at this point. The numerator consists of independent scalar products involving loop and external momenta and possibly transverse vectors, i.e., $k_i \cdot k_j$, $k_i \cdot p_j$, $k_i \cdot \eta_j$. The number N of independent scalar products among loop and external momenta is easily derived, depending on the considered regularization scheme. Denoting with L the number of loops and with E the number of external momenta, in the Conventional Dimensional Regularization (CDR) scheme

$$N = L(L+1)/2 + L(E-1), \quad (2.2)$$

whereas in the t'Hooft-Veltman (tHV) scheme

$$N = \begin{cases} L(L+1)/2 + L(E-1) & \text{for } E < 5 \\ L(L+1)/2 + 4L & \text{for } E \geq 5 \end{cases}. \quad (2.3)$$

¹For the terminology, see Figure 1 of Ref. [93].

²Inverse propagators raised in higher integer powers must also be included to accommodate special contributions.

In one-loop calculations ($L = 1$), the number of inverse propagators n appearing in the denominator of Eq. (2.1) is always larger than or equal to N . Consequently, all scalar products appearing in the numerator \mathcal{N} , besides the so-called spurious terms [79], can be expressed in terms of the inverse propagators D_i , meaning they are all *reducible scalar products* (RSP). Conversely, at higher loops ($L \geq 2$), part of the aforementioned scalar products are not expressible in terms of the D_i 's. The latter are commonly denoted *irreducible scalar products* (ISP).

Extending the OPP approach to two loops, one can express the numerator \mathcal{N} of a generic two-loop integrand in the following form:

$$\mathcal{N} = P^{(n)} + \sum_{i=1}^n P_i^{(n-1)} D_i + \sum_{i=1}^{n-1} \sum_{j>i}^n P_{ij}^{(n-2)} D_i D_j + \dots \quad (2.4)$$

Plugging this expression in Eq. (2.1) results in a splitting of the integrand into terms with a different number of denominators. The quantities $P^{(n)}$, $P_i^{(n-1)}$, $P_{ij}^{(n-2)}$, \dots appearing in Eq. (2.4) are *polynomials* of the form

$$P = \sum_{l=1}^M b_l m_l, \quad (2.5)$$

where $b_i = b_i(\{p\})$ are coefficients which depend on the external kinematics, and the monomials m_i are built upon the ISP characteristic of each term, and possibly of scalar products of the form $k_i \cdot \eta_j$.

Focusing on the two-loop case, our goal is to decompose the amplitude, $\mathcal{A}^{(2)}$, in terms of a set of Feynman integrals F_i and coefficients c_i that depend only on the external kinematics,

$$\mathcal{A}^{(2)} = \sum_i c_i(\{p\}) F_i, \quad (2.6)$$

where the F_i 's take the form

$$F_i \equiv F(a_1, \dots, a_N) = \int \prod_{i=1}^2 [dk_i] \frac{1}{D_1^{a_1} \dots D_N^{a_N}}, \quad a_i \in \mathbb{Z}. \quad (2.7)$$

This can be achieved by appropriately expressing the monomials m_l in Eq. (2.5) in terms of the inverse propagators D_i [94]. Eq. (2.6) is at the core of *numerical* methods for two-loop computations. Provided that the integrals F_i are known (or a procedure to reduce the latter to a subset of master integrals is established), determining the coefficients c_i at *integrand level* helps to address the problem of two-loop computations in a general, process-independent way. This idea expands upon well-established methods developed for one-loop calculations, such as OPP reduction [79].

In the following subsections, we will introduce two different methods that can be used to determine the polynomials P appearing in Eq. (2.4) and to fit their coefficients.

2.2 Linear fit and fit by cut approach

We first address the question of determining the polynomials P and fitting their coefficients in Eq. (2.4), assuming that the numerator is known *analytically*. This allows us to construct the polynomials P directly from the symbolic expressions appearing in the numerator. Moving along the same path of one-loop reduction, the fitting is carried out by iteratively applying cut equations, namely setting denominators to zero. Starting with the so-called maximal cut equation,

$$D_1 = D_2 = \dots = D_n = 0, \quad (2.8)$$

we can identify the coefficients of $P^{(n)}$,

$$P^{(n)} = \mathcal{N}|_{D_1=D_2=\dots=D_n=0}. \quad (2.9)$$

Then we can iteratively fit the rest of the polynomials by appropriately subtracting the terms computed in the previous step. For instance, the first next-to-maximal contribution reads

$$P_1^{(n-1)} = \left(\frac{\mathcal{N} - \mathcal{N}|_{D_1=D_2=\dots=D_n=0}}{D_1} \right) \Big|_{D_2=\dots=D_n=0}, \quad (2.10)$$

and so on. We note that cut equations, Eq. (2.8), translate into a system of linear relations among scalar products $k_i \cdot k_j$ and $k_i \cdot p_j$, where k_i and p_j denote generically loop and external momenta, respectively. This allows us to straightforwardly solve Eq. (2.9), Eq. (2.10), and the rest of the equations resulting from all the sub-maximal cuts, by substitution rules, for any process. We call this procedure of solving Eq. (2.4), a *linear fit*. We will show in the following sections how this applies to the case of 4-, 5-, and 6-particle scattering amplitudes.

In certain instances, the analytical calculation of the numerator \mathcal{N} can prove to be a highly challenging task. In such cases, resorting to a *numerical* computation, facilitated by dedicated software packages such as HELAC-2LOOP [38], can be a feasible alternative. In this case, there are two issues to be addressed:

1. the solutions of cut equations must be expressed in a form suitable for numerical evaluation of numerators;
2. the polynomials P appearing in Eq. (2.4) must be constructed without *a priori* analytical knowledge of the numerator.

To address the first issue, we need a suitable representation of the loop momenta. Given two arbitrary massless momenta l_1^μ, l_2^μ , let us define

$$\begin{aligned} l_3^\mu &= \bar{u}_-(l_1) \gamma^\mu u_-(l_2), \\ l_4^\mu &= \bar{u}_-(l_2) \gamma^\mu u_-(l_1). \end{aligned} \quad (2.11)$$

The set $\{l_1^\mu, l_2^\mu, l_3^\mu, l_4^\mu\}$ forms a basis in $d = 4$ dimensions. This allows us to express the loop momenta k_1, k_2 as follows,

$$\begin{aligned} k_1 &= x_1 l_1^{(1)} + x_2 l_2^{(1)} + x_3 l_3^{(1)} + x_4 l_4^{(1)} \\ k_2 &= y_1 l_1^{(2)} + y_2 l_2^{(2)} + y_3 l_3^{(2)} + y_4 l_4^{(2)} \end{aligned} \quad (2.12)$$

where the coefficients x_i and y_i are expressible in terms of scalar products of the form $k_i \cdot p_j$. The latter coefficients characterize the loop momenta in $d = 4$ dimensions. Complemented by μ_{11} , μ_{12} and μ_{22} ³, they form a set of eleven variables which characterizes completely the loop momenta in $d = 4 - 2\epsilon$ dimensions: $\{x_1, x_2, x_3, x_4, y_1, y_2, y_3, y_4, \mu_{11}, \mu_{12}, \mu_{22}\}$. We solve cut equations⁴ in terms of these variables, as we will see in section 3. In $d = 4 - 2\epsilon$, the solution to the cut equations is unique in terms of the ISP, whereas in $d = 4$ we usually have disjoint branches [46], see section 3.1.1 for an explicit example.

The parametrization of the polynomials P in terms of the ISP is obtained through the program **BasisDet** [46]. The latter provides a set of monomials which take the form $\prod_i x_i^{r_i}$, where x_i denote ISP and r_i is an integer ranging from zero to some upper value calculated from the maximal tensor rank of the polynomial P with respect to k_1 , k_2 and k_1, k_2 combined⁵. For example, a term such as $(k_1 \cdot p_1)^2 (k_2 \cdot p_3)^3$ has a tensor rank 2 for k_1 , 3 for k_2 and 5 for k_1, k_2 combined.

At one loop, P consists of terms depending solely on the external kinematics and the so-called spurious terms, which are specific to each cut. The spurious terms, although necessary for the reduction at the integrand level, do not contribute to the final result as they integrate to zero. The final result is determined by the coefficients that depend only on the external kinematics and multiply the appropriately chosen basis of integrals. At two loops, the existence of spurious terms that integrate to zero is less straightforward: there are certainly spurious terms compiled by the loop momenta and the transverse directions over the external momenta, whenever present. Nevertheless, the simple one-loop picture is spoiled by the fact that the integrals in Eq. (2.7) obey a set of IBP identities, resulting in a set of master integrals, which are then evaluated using different techniques. In this paper, we do not address the issue of IBP reduction: we assume that all the integrals resulting from the integrand reduction are, or will be, available numerically, as happens for the one-loop case.

Returning to the solution of Eq. (2.4), let us first address the case of $d = 4 - 2\epsilon$ dimensions. The cut equations fix a subset of the eleven parameters needed to fully describe the loop momenta. Assuming that the set of monomials m_i ($i = 1, \dots, M$) parametrizing a given polynomial P is established, then an $M \times M$ matrix, \mathcal{M} , is obtained by evaluating the monomials on the solution to the cut equation, by assigning random values to its free parameters. The numerator can be cast in the form

$$\mathcal{N} = \mathcal{N}_4 + \sum \epsilon^i \mathcal{N}_\epsilon^{(i)}, \quad (2.13)$$

where both $\mathcal{N}_4 = \mathcal{N}|_{d=4}$ and $\mathcal{N}_\epsilon^{(i)}$ are accessible numerically and explicitly depending on μ_{ij} . These terms are used to calculate, with the same random values, the $M \times 1$ matrices $\mathcal{B}^{(4)}$, $\mathcal{B}^{(i)}$. Then the given polynomial P is written explicitly as

$$P = \sum_{i=1}^M \left(c_i^{(d=4)} + \sum \epsilon^j c_i^{(j)} \right) m_i \quad (2.14)$$

³In $d = 4 - 2\epsilon$, $\mu_{ij} \equiv k_i^{(\epsilon)} \cdot k_j^{(\epsilon)}$, with $k^{(\epsilon)}$ the components of the loop momenta beyond $d = 4$ dimensions.

⁴For alternative approaches, see Refs. [44–47, 52, 53].

⁵Corresponding to **RenormalizationCondition** in ref. [46].

where

$$\vec{c}^{(d=4)} = \mathcal{M}^{-1} \mathcal{B}^{(4)} \quad \vec{c}^{(i)} = \mathcal{M}^{-1} \mathcal{B}^{(i)} \quad (2.15)$$

After the whole iterative procedure is completed, the so-called $N = N$ test is performed. The latter consists of checking the validity of Eq. (2.4) for arbitrary assignment of numerical values for all free parameters of the loop kinematics. We have checked that the $N = N$ test is fulfilled when the polynomials P are constructed directly from the analytic expression of the numerator, as well as when using **BasisDet** to construct the ansatz for the polynomials.

In $d = 4$ we obtain several disjoint solutions of the cut equations. On each branch, we have checked analytically that the $d = 4$ numerator assumes a different form. On the other hand, the set of monomials obtained previously in $d = 4 - 2\epsilon$ dimensions, contains linear dependencies due to the fact that in $d = 4$ the two loop momenta and the three independent external momenta in a 4-particle amplitude for instance, is an over complete set and Gram determinants among them vanish, leading to non-trivial relations. In that case, the set of monomials m_i , provided by **BasisDet**, is evaluated at each branch of the cut-equation solution. Assuming the existence of r branches, the matrix \mathcal{M} has size $(rM) \times M$ and $\mathcal{B}_0^{(4)}$, sized $(rM) \times 1$, is calculated using $\mathcal{N}_{4,0} = \mathcal{N}|_{\mu_{ij}=0, d=4}$. The system

$$\mathcal{M} \vec{c}^{(d=4)} = \mathcal{B}_0^{(4)} \quad (2.16)$$

can still be solved with standard Linear Algebra algorithms such as QR decomposition, as long as the rank of the matrix is full, namely $\text{rank}(\mathcal{M}) = M$. As we will see later, this is true in most cases, but solutions can still be obtained in cases where the matrix is rank-deficient, $\text{rank}(\mathcal{M}) < M$. Notice that although in $d = 4 - 2\epsilon$ case the reduction of the amplitude is complete, in $d = 4$, the so-called rational terms need to be calculated [95–99].

2.3 Global fit approach

Assuming that the numerator \mathcal{N} is a function of the eleven (eight) parameters in $d = 4 - 2\epsilon$ ($d = 4$) dimensions, and a numerator provider (such as **HELAC-2LOOP**) is capable of returning numerical values for \mathcal{N}_4 and \mathcal{N}_ϵ , we can instead determine all the coefficients of a single polynomial P by means of a *global fit* [17, 55]. In this method, all monomials involved in the polynomial P are evaluated for several arbitrary random numerical assignments of the above-mentioned parameters. In this way, we construct a single square matrix \mathcal{M} , with size $M \times M$, where M is the number of the monomials appearing in P . Using the same random values of the parameters, we also sample the numerator functions \mathcal{N}_4 , \mathcal{N}_ϵ , $\mathcal{N}_{4,0}$ and build $M \times 1$ matrices that we denote $\mathcal{B}^{(4)}$, $\mathcal{B}^{(\epsilon)}$ and $\mathcal{B}_0^{(4)}$ respectively. The difference to the fit by cut approach is that the kinematics are not constrained to obey cut equations. While the number M of monomials is much larger, since it accommodates all monomials from all polynomials in Eq. (2.4), there are no significant conceptual differences between the two approaches. As we will show later, the solution can be obtained by using standard Linear Algebra packages, such as **Eigen** [100] and **LAPACK** [101], at both double and quadruple precision.

2.4 Projecting over a full family

From the perspective of the one-loop OPP approach, Eq. (2.4) addresses the reduction of the numerator in Eq. (2.1) in terms of the n inverse propagators D_i appearing in it. As we already pointed out, the one-loop case is special in the sense that the number of independent scalar products N and the number of inverse propagators n obey the relation $N \leq n$. Thus, all scalar products can be expressed in terms of the D_i 's, which appear in the denominator of the loop integrand. Starting from two loops, $N > n$, and thus one is left with a set of ISP that cannot be expressed as above. However, one can define an enlarged set of inverse propagators such that *all* scalar products are expressible as combinations of the latter. This enlarged set of inverse propagators is named *family*. We can consider projecting the numerator over the full family of inverse propagators:

$$\mathcal{N} = P^{(N)} + \sum_{i=1}^N P_i^{(N-1)} D_i + \sum_{i=1}^{N-1} \sum_{j>i}^N P_{ij}^{(N-2)} D_i D_j + \dots \quad (2.17)$$

For example, cutting over 7 propagators in a two-loop four-particle topology,

$$\begin{aligned} \mathcal{N}_{4p} = & P_{7c}(v_1, v_2, u_1, u_2) + \sum_{i=1}^7 P_{6c}^{(i)}(v_1, v_2, u_1^i, u_2^i, u_3^i) D_i \\ & + \sum_{i<j}^7 P_{5c}^{(i,j)}(v_1, v_2, u_1^{i,j}, u_2^{i,j}, u_3^{i,j}, u_4^{i,j}) D_i D_j \\ & + \sum_{i<j<k}^7 P_{4c}^{(i,j,k)}(v_1, v_2, u_1^{i,j,k}, \dots, u_5^{i,j,k}) D_i D_j D_k \\ & + \sum_{i<j<k<l}^7 P_{3c}^{(i,j,k,l)}(v_1, v_2, u_1^{i,j,k,l}, \dots, u_6^{i,j,k,l}) D_i D_j D_k D_l \\ & + \sum_{i<j<k<l<m}^7 P_{2c}^{(i,j,k,l,m)}(v_1, v_2, u_1^{i,j,k,l,m}, \dots, u_7^{i,j,k,l,m}) D_i D_j D_k D_l D_m + \dots \end{aligned} \quad (2.18)$$

will generically lead to polynomials P depending on more variables rather than cutting over all 9 propagators,

$$\begin{aligned} \mathcal{N}_{4p} = & P_{9c}(v_1, v_2) + \sum_{i=1}^9 P_{8c}^{(i)}(v_1, v_2, u_i) D_i + \sum_{i<j}^9 P_{7c}^{(i,j)}(v_1, v_2, u_i, u_j) D_i D_j \\ & + \sum_{i<j<k}^9 P_{6c}^{(i,j,k)}(v_1, v_2, u_i, u_j, u_k) D_i D_j D_k \\ & + \sum_{i<j<k<l}^9 P_{5c}^{(i,j,k,l)}(v_1, v_2, u_i, u_j, u_k, u_l) D_i D_j D_k D_l \\ & + \sum_{i<j<k<l<m}^9 P_{4c}^{(i,j,k,l,m)}(v_1, v_2, u_i, u_j, u_k, u_l, u_m) D_i D_j D_k D_l D_m + \dots \end{aligned} \quad (2.19)$$

In the previous equations, $v_i \equiv k_i \cdot \eta$, where η is the vector transverse to p_1, p_2, p_3 necessary to complete the 4-dimensional physical space, while $u_I, u_I^i, u_I^{i,j}, u_I^{i,j,k}, u_I^{i,j,k,l}, \dots$, stand for ISP in the corresponding cut.

The same is true for a five-particle amplitude, where cutting over 8 propagators results in

$$\begin{aligned}
\mathcal{N}_5 = & P_{8c}(u_1, u_2, u_3) + \sum_{i=1}^8 P_{7c}^{(i)}(u_1^i, \dots, u_4^i) D_i \\
& + \sum_{i<j}^8 P_{6c}^{(i,j)}(u_1^{i,j}, \dots, u_5^{i,j}) D_i D_j \\
& + \sum_{i<j<k}^8 P_{5c}^{(i,j,k)}(u_1^{i,j,k}, \dots, u_6^{i,j,k}) D_i D_j D_k \\
& + \sum_{i<j<k<l}^8 P_{4c}^{(i,j,k,l)}(u_1^{i,j,k,l}, \dots, u_7^{i,j,k,l}) D_i D_j D_k D_l \\
& + \sum_{i<j<k<l<m}^8 P_{3c}^{(i,j,k,l,m)}(u_1^{i,j,k,l,m}, \dots, u_8^{i,j,k,l,m}) D_i D_j D_k D_l D_m + \dots
\end{aligned} \tag{2.20}$$

while cutting over all 11 propagators, which defines the 5-point family, results in

$$\begin{aligned}
\mathcal{N}_5 = & P_{11c} + \sum_{i=1}^{11} P_{10c}^{(i)}(u_i) D_i + \sum_{i<j}^{11} P_{9c}^{(i,j)}(u_i, u_j) D_i D_j \\
& + \sum_{i<j<k}^{11} P_{8c}^{(i,j,k)}(u_i, u_j, u_k) D_i D_j D_k \\
& + \sum_{i<j<k<l}^{11} P_{7c}^{(i,j,k,l)}(u_i, u_j, u_k, u_l) D_i D_j D_k D_l \\
& + \sum_{i<j<k<l<m}^{11} P_{6c}^{(i,j,k,l,m)}(u_i, u_j, u_k, u_l, u_m) D_i D_j D_k D_l D_m + \dots
\end{aligned} \tag{2.21}$$

Notice that in this case P_{11c} depends only on the external kinematics, since the maximal cut determines all degrees of freedom of the loop momenta. We observe that projecting over the full family has the effect of simplifying the structure of the individual polynomials P , since they depend on a reduced number of ISP. Moreover, all the ISP u_i in Eq. (2.21), can be expressed in terms of the inverse propagators of the family, leading directly to a variation of the master equation,

$$\mathcal{N}_5 = c^{(0)} + \sum_{i=1}^{11} \sum_a c^{(i,a)} D_i^a + \sum_{i<j}^{11} \sum_{a,b} c^{(i,j,a,b)} D_i^a D_j^b + \dots \tag{2.22}$$

where, first the coefficients c depend only on the external kinematics and second the inverse Feynman propagators, D_i , enter not linearly as before, but with powers determined by the

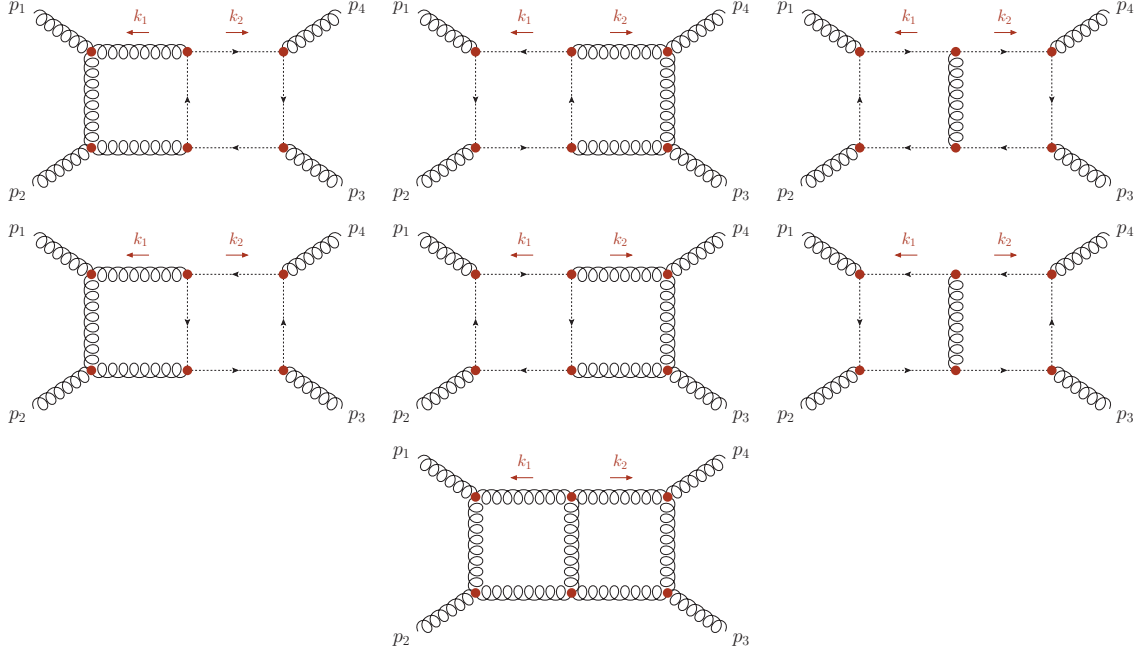


Figure 1: Feynman graphs contributing to the double-box numerator under study. There are seven contributions, considering gluons and (anti-)ghosts running within the loops. Curly lines denote gluons, while dotted lines denote ghosts (arrow aligned with the momentum flow) and anti-ghosts (arrow in the opposite direction of the momentum flow).

fit-by-cut procedure. The amplitude is then given by,

$$\mathcal{A}_5^{(2)} = c^{(0)} F[a_1, \dots, a_{11}] + \sum_{i=1}^{11} \sum_a c^{(i,a)} F[a_1, \dots, a_i - a, \dots, a_{11}] + \dots \quad (2.23)$$

with $a_1 = \dots = a_8 = 1$ and $a_9 = a_{10} = a_{11} = 0$ and F given as in Eq.(2.7). Eqs. (2.20-2.23) are straightforwardly extensible to any n -particle amplitude with $n > 5$, see section 3.3.1 for details in case $n = 6$.

3 Application of the method

In this section, the application of the method described in section 2 is demonstrated through several examples. The considered numerators are representative of a variety of scattering processes and consist of different kinematic dependencies, ranging from four-point to six-point kinematics. For the generation of the analytic expressions required, we used the *Mathematica* packages *FeynArts* [35] and *FeynCalc* [102], except for the 6-particle case, section 3.3.1, which has been generated by *FORM* [103].

3.1 Four-Point Kinematics

3.1.1 Double-box topologies

Here we focus on the numerator of the double-box topology constructed by the seven Feynman graphs depicted in Fig. 1. This numerator contributes to the scattering amplitude of the process $gg \rightarrow gg$. The inverse propagators describing the family for this topology can be chosen as

$$\begin{aligned} D_1 &= k_1^2, & D_2 &= (k_1 + p_1)^2, & D_3 &= (k_1 + p_{12})^2, & D_4 &= (k_1 + k_2)^2, & D_5 &= k_2^2, \\ D_6 &= (k_2 - p_{123})^2, & D_7 &= (k_2 - p_{12})^2, & D_8 &= (k_2 - p_1)^2, & D_9 &= (k_1 + p_{123})^2 \end{aligned} \quad (3.1)$$

Above and henceforth, the shorthand notation $p_{i\dots j} = p_i + \dots + p_j$ will be used to denote the sum of the incoming external momenta, and $s = (p_1 + p_2)^2$ and $t = (p_2 + p_3)^2$ the standard Mandelstam variables. For all analyses presented below, we have used the following helicity assignment: $\lambda_1 = +1, \lambda_2 = +1, \lambda_3 = -1, \lambda_4 = -1$, for the helicities of the external gluons, all assumed to be incoming.

1. Linear fit

We seek to solve Eq. (2.18) using cut equations and the known analytic expression of the numerator.

The maximal cut equations

$$D_1 = D_2 = D_3 = D_4 = D_5 = D_6 = D_7 = 0 \quad (3.2)$$

result in determining seven invariants

$$\begin{aligned} k_1 \cdot k_1 &\rightarrow 0, & k_1 \cdot k_2 &\rightarrow 0, & k_1 \cdot p_1 &\rightarrow 0, & k_1 \cdot p_2 &\rightarrow -\frac{s}{2}, & k_2 \cdot k_2 &\rightarrow 0, \\ k_2 \cdot p_2 &\rightarrow \frac{s}{2} - k_2 \cdot p_1, & k_2 \cdot p_3 &\rightarrow -\frac{s}{2}. \end{aligned} \quad (3.3)$$

By applying the above relation on both sides of Eq. (2.18), we can fully determine the polynomial P_7 . The latter consists of 70 coefficients over the ISP monomials $\{k_1 \cdot p_3, k_1 \cdot \eta, k_2 \cdot p_1, k_2 \cdot \eta\}$.

Subtracting P_7 in Eq. (2.18), we can now determine the polynomials of kind P_6 in the same way. There are seven six-cuts and therefore seven P_6 polynomials to determine. As an example, the first six-cut,

$$D_2 = D_3 = D_4 = D_5 = D_6 = D_7 = 0 \quad (3.4)$$

leads to

$$\begin{aligned} k_2 \cdot p_2 &\rightarrow \frac{s}{2} - k_2 \cdot p_1, & k_1 \cdot p_2 &\rightarrow -\frac{s}{2}, & k_2 \cdot p_3 &\rightarrow -\frac{s}{2}, \\ k_1 \cdot k_2 &\rightarrow k_1 \cdot p_1, & k_1 \cdot k_1 &\rightarrow -2k_1 \cdot p_1, & k_2 \cdot k_2 &\rightarrow 0, \end{aligned} \quad (3.5)$$

where there are now 5 ISP: $\{k_1 \cdot p_2, k_1 \cdot p_3, k_1 \cdot \eta, k_2 \cdot p_1, k_2 \cdot \eta\}$. The polynomial $P_1^{(6)}$ consists of 111 coefficients. This process is iterated until the level of a two-cut,

Level	Number of cuts	Number of coefficients	Scaling
7	1	70	4,4,4
6	7	695	3,3,4
5	21	1430	3,3,3
4	35	1017	2,2,2
3	35	225	1,1,1
2	21	9	0,0,0

Table 1: Double-box linear fit information beginning with 7-cut. The numbers in the last column refer to the maximum powers of k_1 , k_2 , and k_1, k_2 combined, as described in the text.

after which all resulting polynomials vanish. The data for all cuts are summarized in Tab. 1. The analytic solution for the polynomials satisfies explicitly Eq. (2.18).

We now seek to solve Eq. (2.19), namely projecting over all 9 propagators in the double-box family. This has the advantage of building a reduction procedure that covers all 4-particle planar diagrams, including the double-box, the penta-triangle and the hexa-bubble. The maximal cut equations read

$$D_1 = D_2 = D_3 = D_4 = D_5 = D_6 = D_7 = D_8 = D_9 = 0 \quad (3.6)$$

which leads to

$$\begin{aligned} k_1 \cdot k_1 \rightarrow 0, \quad k_1 \cdot k_2 \rightarrow 0, \quad k_1 \cdot p_1 \rightarrow 0, \quad k_1 \cdot p_2 \rightarrow -\frac{s}{2}, \quad k_1 \cdot p_3 \rightarrow \frac{s}{2}, \\ k_2 \cdot k_2 \rightarrow 0, \quad k_2 \cdot p_1 \rightarrow 0, \quad k_2 \cdot p_2 \rightarrow \frac{s}{2}, \quad k_2 \cdot p_3 \rightarrow -\frac{s}{2} \end{aligned} \quad (3.7)$$

By applying the above relations on both sides of Eq. (2.19), we can fully determine the polynomial P_9 . The latter consists of 13 coefficients over the ISP monomials $\{k_1 \cdot \eta, k_2 \cdot \eta\}$. Subtracting as before P_9 in Eq. (2.19), we can now determine the polynomials P_8 in the same way. There are nine 8-cuts and therefore nine P_8 polynomials to determine. As an example, the first 8-cut,

$$D_2 = D_3 = D_4 = D_5 = D_6 = D_7 = D_8 = D_9 = 0 \quad (3.8)$$

leads to

$$\begin{aligned} k_2 \cdot p_1 \rightarrow 0, \quad k_2 \cdot p_2 \rightarrow \frac{s}{2}, \quad k_1 \cdot p_2 \rightarrow -\frac{s}{2}, \quad k_2 \cdot p_3 \rightarrow -\frac{s}{2}, \quad k_1 \cdot p_3 \rightarrow \frac{s}{2}, \\ k_1 \cdot k_2 \rightarrow k_1 \cdot p_1, \quad k_1 \cdot k_1 \rightarrow -2k_1 \cdot p_1, \quad k_2 \cdot k_2 \rightarrow 0, \end{aligned} \quad (3.9)$$

where there are now 3 ISP: $\{k_1 \cdot p_1, k_1 \cdot \eta, k_2 \cdot \eta\}$.

The data for all cuts are summarized in Tab. 2. The analytic solutions for the polynomials satisfy explicitly Eq. (2.18). The total number of non-zero coefficients is slightly larger than previously, namely 3544 versus 3446. We have verified that after reducing

Level	Number of cuts	Number of coefficients	Scaling
9	1	13	4,4,4
8	9	227	4,4,4
7	36	963	3,3,3
6	84	1445	2,2,2
5	126	780	1,1,1
4	126	116	0,0,0

Table 2: Double-box linear fit information beginning with 9-cut.

by IBP identities the integrals appearing in Eqs. (2.18,2.19), the coefficients of the top-sector master integrals coincide with those obtained from `Caravel` [56], for all helicity assignments ⁶

2. Fit by cut in $d = 4 - 2\epsilon$ dimensions

Let us now assume that the numerator is available only using a numerical approach, as the one implemented in `HELAC-2LOOP`, including terms proportional to μ_{ij} and $\epsilon = (d - 4)/2$. Then the realization of the solutions of the cut equations, Eq. (3.3) in a numerical setup is based on the determination of the four-dimensional part of the loop momenta following Eq. (2.12). In fact the solution for any cut has a unique analytic form in terms of ISP. The 7 cut, Eq. (3.3), reads as follows:

$$\begin{aligned}
k_1 \cdot p_1 &\rightarrow 0, & k_2 \cdot p_2 &\rightarrow \frac{1}{2}(s - 2k_2 \cdot p_1), & k_1 \cdot p_2 &\rightarrow -\frac{s}{2}, & k_2 \cdot p_3 &\rightarrow -\frac{s}{2}, \\
\mu_{11} &\rightarrow -\frac{\frac{4s(k_1 \cdot p_3)^2}{s+t} - 4sk_1 \cdot p_3 + 4t(k_1 \cdot \eta)^2 + s(s+t)}{4t}, \\
\mu_{12} &\rightarrow \frac{\frac{k_1 \cdot p_3(4(s+2t)k_2 \cdot p_1 - 2st)}{s+t} + t(s - 4k_1 \cdot \eta k_2 \cdot \eta) - 2sk_2 \cdot p_1}{4t}, \\
\mu_{22} &\rightarrow -\frac{4stk_2 \cdot p_1 + 4s(k_2 \cdot p_1)^2 + t(4(s+t)(k_2 \cdot \eta)^2 + st)}{4t(s+t)}
\end{aligned} \tag{3.10}$$

For comparison, the cut conditions for 9 propagators are

$$\begin{aligned}
k_2 \cdot p_1 &\rightarrow 0, & k_1 \cdot p_1 &\rightarrow 0, & k_2 \cdot p_2 &\rightarrow \frac{s}{2}, & k_1 \cdot p_2 &\rightarrow -\frac{s}{2}, \\
k_2 \cdot p_3 &\rightarrow -\frac{s}{2}, & k_1 \cdot p_3 &\rightarrow \frac{s}{2}, & \mu_{11} &\rightarrow -(k_1 \cdot \eta)^2 - \frac{st}{4(s+t)}, \\
\mu_{12} &\rightarrow \frac{st}{4(s+t)} - k_1 \cdot \eta k_2 \cdot \eta, & \mu_{22} &\rightarrow -(k_2 \cdot \eta)^2 - \frac{st}{4(s+t)}
\end{aligned} \tag{3.11}$$

⁶In `Caravel` the results are given for the color-stripped helicity amplitude, whereas in our case we have studied a subset of the contributions to the amplitude, as given in Fig. 1. Nevertheless, a comparison of the top-sector master integral coefficients is possible since all other Feynman graphs do not contribute to them.

Level	RenormalizationCondition
7	$\{\{\{1,0\},4\},\{\{0,1\},4\},\{\{1,1\},4\}\}$
6	$\{\{\{1,0\},4\},\{\{0,1\},4\},\{\{1,1\},4\}\}$
5	$\{\{\{1,0\},3\},\{\{0,1\},3\},\{\{1,1\},3\}\}$
4	$\{\{\{1,0\},2\},\{\{0,1\},2\},\{\{1,1\},2\}\}$
3	$\{\{\{1,0\},1\},\{\{0,1\},1\},\{\{1,1\},1\}\}$
2	$\{\{\{1,0\},0\},\{\{0,1\},0\},\{\{1,1\},0\}\}$

Table 3: Max Power for k_1 , k_2 and k_1 , k_2 combined, used as inputs for **BasisDet**.

In terms of the basis introduced in section 2.2, *i.e.* $\{x_1, \dots, x_4, y_1, \dots, y_4, \mu_{11}, \mu_{12}, \mu_{22}\}$, the solution takes the form

$$\begin{aligned} x_1 \rightarrow -1, \quad x_2 \rightarrow 0, \quad y_1 \rightarrow 0, \quad y_2 \rightarrow -1, \quad \mu_{11} \rightarrow 4sx_3x_4, \quad \mu_{22} \rightarrow 4sy_3y_4, \\ \mu_{12} \rightarrow (x_3 + x_4 - y_3 - y_4)r - 2(s+t)(x_4y_4 + x_3y_3) - 2t(x_3y_4 + x_4y_3) - t/2 \end{aligned} \quad (3.12)$$

with $r = \sqrt{-t(s+t)}$. In a numerical setup, for instance, calculating on the kinematic point $s = 1$, $t = -1/5$, the 7-cut is represented by

$$\begin{aligned} x_1 \rightarrow -1, \quad x_2 \rightarrow 0, \quad y_1 \rightarrow 0, \quad y_2 \rightarrow -1, \quad \mu_{11} \rightarrow 4x_3x_4, \quad \mu_{22} \rightarrow 4y_3y_4, \\ \mu_{12} \rightarrow (4x_3(-4y_3 + y_4 + 1) + 4x_4(y_3 - 4y_4 + 1) - 4y_3 - 4y_4 + 1)/10 \end{aligned} \quad (3.13)$$

We can now determine the coefficients of the polynomial P_7 , which in this case has 70 coefficients, by calculating the numerator and the monomials of the basis, using 70 random assignments of the undetermined variables, x_3, x_4, y_3, y_4 , and solving the corresponding matrix equation

$$\sum_{j=1}^{70} M_{ij} c_j = \mathcal{N}_i, \quad i = 1, \dots, 70 \quad (3.14)$$

for the unknown coefficients c . The full-rank matrix M is straightforwardly invertible, and the solution checked agrees to the numerical precision used against the analytic result. We have confirmed that this way we can calculate all the coefficients of Tab. 1 numerically. The same is true for the case of projecting over the 9 propagators, see Tab. 2.

3. Fit by cut in $d = 4$ dimensions

In this case, the monomials that make up the polynomials of the analytic solution described either by the linear fit or the fit by cut in $d = 4 - 2\epsilon$, are not independent, due to the existence of Gram-determinant identities which hold in $d = 4$ dimensions. This is why for $d = 4$ we use **BasisDet** as a means to parametrize the polynomials, therefore no longer relying on analytical knowledge of the numerator in order to create the ansatz. By construction, this requires us to specify the highest powers of the loop momenta to the **BasisDet** program. Following the data of Tab. 1, the so-called RenormalizationCondition in **BasisDet** is fixed as shown in Tab. 3. Contrary

to the $d = 4 - 2\epsilon$ case discussed previously, in $d = 4$ the cut equations do not admit a unique solution in terms of ISP. Using the same values for s, t as above, the 7-cut solution is split into 6 branches,

$$\begin{aligned} & \left\{ x_1 \rightarrow -1, x_2 \rightarrow 0, x_3 \rightarrow 0, x_4 \rightarrow \frac{4y_3 - 1}{4(y_3 + 1)}, y_1 \rightarrow 0, y_2 \rightarrow -1, y_4 \rightarrow 0, y_3 \rightarrow z(1) \right\}, \\ & \left\{ x_1 \rightarrow -1, x_2 \rightarrow 0, x_3 \rightarrow \frac{4y_4 - 1}{4(y_4 + 1)}, x_4 \rightarrow 0, y_1 \rightarrow 0, y_2 \rightarrow -1, y_3 \rightarrow 0, y_4 \rightarrow z(1) \right\}, \\ & \left\{ x_1 \rightarrow -1, x_2 \rightarrow 0, x_3 \rightarrow 0, x_4 \rightarrow -\frac{1}{4}, y_1 \rightarrow 0, y_2 \rightarrow -1, y_3 \rightarrow 0, y_4 \rightarrow z(1) \right\}, \\ & \left\{ x_1 \rightarrow -1, x_2 \rightarrow 0, x_3 \rightarrow -\frac{1}{4}, x_4 \rightarrow 0, y_1 \rightarrow 0, y_2 \rightarrow -1, y_4 \rightarrow 0, y_3 \rightarrow z(1) \right\}, \\ & \left\{ x_1 \rightarrow -1, x_2 \rightarrow 0, x_3 \rightarrow 0, y_1 \rightarrow 0, y_2 \rightarrow -1, y_3 \rightarrow 0, y_4 \rightarrow \frac{1}{4}, x_4 \rightarrow z(1) \right\}, \\ & \left\{ x_1 \rightarrow -1, x_2 \rightarrow 0, x_4 \rightarrow 0, y_1 \rightarrow 0, y_2 \rightarrow -1, y_3 \rightarrow \frac{1}{4}, y_4 \rightarrow 0, x_3 \rightarrow z(1) \right\}, \end{aligned}$$

each one parametrized by one undetermined variable $z(1)$. The polynomial P_7 is parametrized by only 28 coefficients, in $d = 4$. By assigning 28 random values to $z(1)$ for each solution, we may form a matrix equation as follows:

$$\sum_{j=1}^{28} M_{ij} c_j = \mathcal{N}_i, \quad i = 1, \dots, 168 \quad (3.15)$$

where the rows of the matrix M consist of the values of the monomials involved in the basis and \mathcal{N} are the corresponding values of the numerator. Although this is a rectangular system of equations, it admits a unique solution for the coefficients c . We have checked against the analytic solution and found agreement up to the numerical precision used. The same is true for all lower-level cuts.

4. Global fit in $d = 4 - 2\epsilon$ dimensions

As an alternative to determining the structure of Eq. (2.18), through cut equations, we have also studied the global fit, as described in the previous section. By expressing both sides of Eq. (2.18) in terms of the variables $V = \{x_1, x_2, x_3, x_4, y_1, y_2, y_3, y_4, \mu_{11}, \mu_{12}, \mu_{22}\}$, parameterizing the loop momenta, we can form a matrix equation over all undetermined parameters c entering in the definition of the polynomials P_7, \dots, P_2 in Eq. (2.18). The number of parameters c , as well as the monomials involved, is 3446. Assigning random values to all 11 variables of V , we form the equation

$$\sum_{j=1}^{3446} M_{ij} c_j = \mathcal{N}_i, \quad i = 1, \dots, 3446 \quad (3.16)$$

where, as before, M is the matrix formed by the numerical values of the monomials and \mathcal{N} the numerical values of the numerator. The matrix M is of full rank and the solution has been determined both in **Mathematica** as well as using purely numerical

tools, such as **Eigen** and **LAPACK**. In fact, the latter offers us the possibility to obtain our results in both double and quadruple precision. As a check of the validity of the solution, the $N = N$ test is successfully performed, in full precision, for arbitrary random assignment of the variables in V .

5. Global fit in $d = 4$ dimensions

A global fit in $d = 4$ can be performed following the same line of reasoning as before. The total number of coefficients c and monomials is 3018. The variables describing the loop momenta are $V = \{x_1, x_2, x_3, x_4, y_1, y_2, y_3, y_4\}$. Assigning random values to all 8 variables of V , we form the equation

$$\sum_{j=1}^{3018} M_{ij} c_j = \mathcal{N}_i, \quad i = 1, \dots, 3018 \quad (3.17)$$

where as before M is the matrix formed by the numerical values of the monomials and \mathcal{N} the numerical values of the numerator in $d = 4$ dimensions. The matrix M is of full rank and the solution has been determined both in **Mathematica** as well as using purely numerical engines, such as **Eigen** and **LAPACK**. In fact the numerical engines offer us the possibility to obtain our results in both double and quadruple precision. As a check of the validity of the solution, the $N = N$ test is successfully performed, in full precision, for arbitrary random assignment of the variables in V .

3.1.2 Penta-triangle topologies

In this subsection, we study the numerator of the penta-triangle topology produced by the seven Feynman graphs depicted in Fig. 2. This numerator is part of the scattering amplitude of the process $gg \rightarrow gg$. The helicity assignment is as in the case of double-box. The propagators describing the family for this topology coincide with the ones of Eq. (3.1), but we choose a different ordering such that the auxiliary propagators appear in the end

$$D_1 = k_1^2, \quad D_2 = (k_1 + p_1)^2, \quad D_3 = (k_1 + p_{12})^2, \quad D_4 = (k_1 + p_{123})^2, \quad D_5 = (k_1 + k_2)^2, \\ D_6 = k_2^2, \quad D_7 = (k_2 - p_{123})^2, \quad D_8 = (k_2 - p_{12})^2, \quad D_9 = (k_2 - p_1)^2$$

1. Linear fit, fit by cut, and global fit in $d = 4 - 2\epsilon$ dimensions

The $d = 4 - 2\epsilon$ analysis is producing the same qualitative results as in the double-box case. For instance, the 7-cut is given by

$$k_1 \cdot k_1 \rightarrow 0, \quad k_1 \cdot k_2 \rightarrow 0, \quad k_1 \cdot p_1 \rightarrow 0, \quad k_1 \cdot p_2 \rightarrow -\frac{s}{2}, \quad k_1 \cdot p_3 \rightarrow \frac{s}{2}, \quad (3.18) \\ k_2 \cdot k_2 \rightarrow 0, \quad k_2 \cdot p_3 \rightarrow -(k_2 \cdot p_1) - k_2 \cdot p_2$$

The data regarding the number of cuts, coefficients of polynomials, and respective powers are collected in Tab. 4.

The corresponding data when projecting over 9 propagators are shown in Tab. 5.

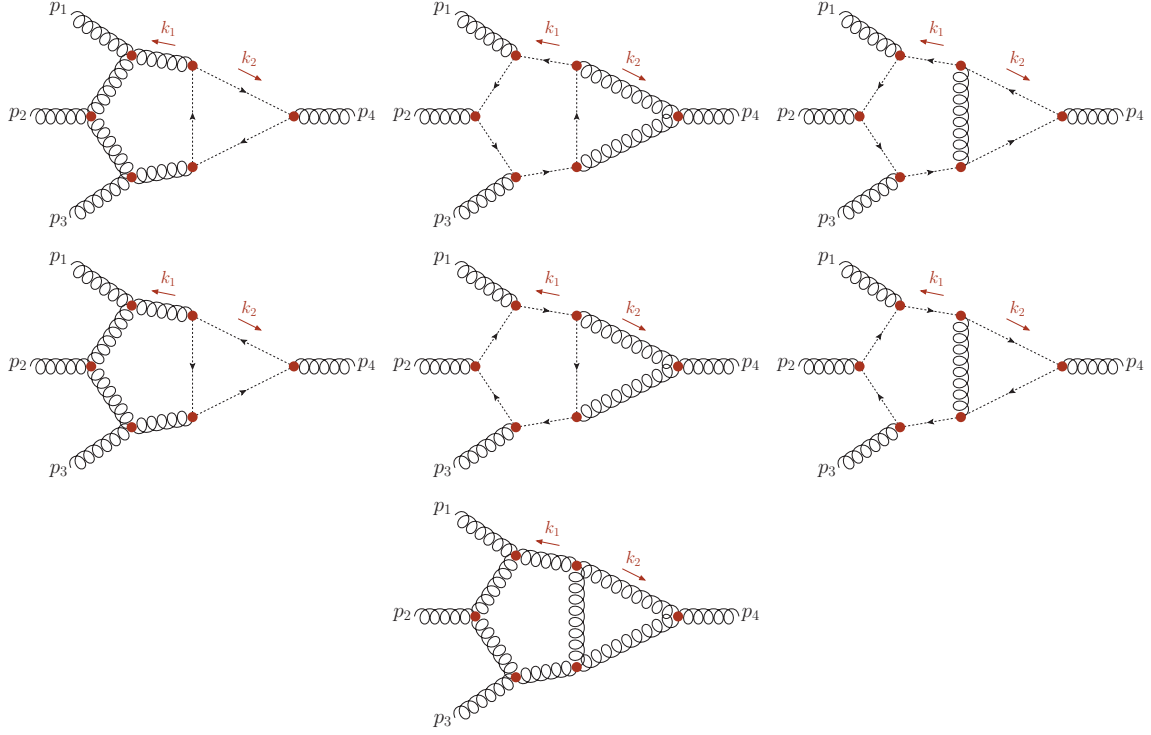


Figure 2: Feynman graphs contributing to the penta-triangle numerator under study. There are seven contributions, considering gluons and (anti-)ghosts running within the loops.

Level	Number of cuts	Number of coefficients	Scaling
7	1	53	4,4,4
6	7	573	4,4,4
5	21	1249	3,3,3
4	35	929	2,2,2
3	35	206	1,1,1
2	21	8	0,0,0

Table 4: Penta-triangle linear fit information beginning with 7-cut.

2. Fit by cut and global fit $d = 4$

In $d = 4$, as before, we have to rely on **BasisDet** in order to construct monomial bases. In this case, the numerator evaluated on all 7-cut solutions is zero. In the 6-cut sector, a new issue arises, namely, there are cuts for which the corresponding matrix equation, see Eq. (3.15), is rank deficient, meaning that the solution is described in terms of undetermined coefficients. These undetermined coefficients, however, do not impact the $N = N$ test. The same is true for the global fit, see Eq. (3.17), where again the equation is rank deficient, nevertheless, its solution correctly describes the numerator. We note that the penta-triangle is the only case studied in this paper where such a

Level	Number of cuts	Number of coefficients	Scaling
7	1	9	3,3,3
6	9	573	4,3,4
5	36	899	3,3,3
4	84	1279	2,2,2
3	126	652	1,1,1
2	126	100	0,0,0

Table 5: Penta-triangle linear fit information beginning with 9 cut.

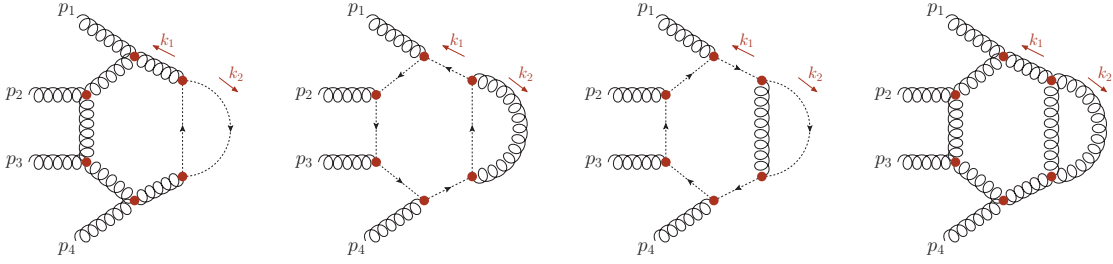


Figure 3: Feynman graphs contributing to the hexa-bubble numerator under study. There are four contributions, considering gluons and (anti-)ghosts running within the loops.

problem occurs.

This presents quite an interesting theoretical challenge for the construction of the ansatz: On the one hand, we have verified that choosing a loose ansatz, meaning a polynomial that leads to a rank deficient matrix is in fact not a problem, as long as the system is still solvable and the $N = N$ test is not affected. This may continue to hold if one chooses a polynomial basis which leads to an unsolvable linear equation, which we also found to be a potential pitfall during our study of this particular topology in $d = 4$. On the other hand, restricting oneself to a smaller basis of polynomials, meaning polynomials containing a very small number of monomials can lead to the following problem: While the solution to the linear equation may even be unique (i.e. full rank of the matrix \mathcal{M}), the functional behavior of the numerator may not be properly accounted for, leading to an incorrect solution which does not reproduce the $N = N$ test. The issue, therefore, of choosing an ansatz, i.e., a proper basis of polynomials to describe a given numerator is not at all trivial and still somewhat remains an open question, especially important if one aims to perform a $d = 4$ fit. While **BasisDet** seems to be the best option available, it still runs the risk of falling into one of the two above problems, depending on the inputs given.

3.1.3 Hexa-bubble topologies

We now consider the numerator of the hexa-bubble topology consisting of the four Feynman graphs depicted in Fig. 3. This numerator is part of the scattering amplitude of the process $gg \rightarrow gg$. The helicity assignment is as in the case of double-box. The inverse propagators

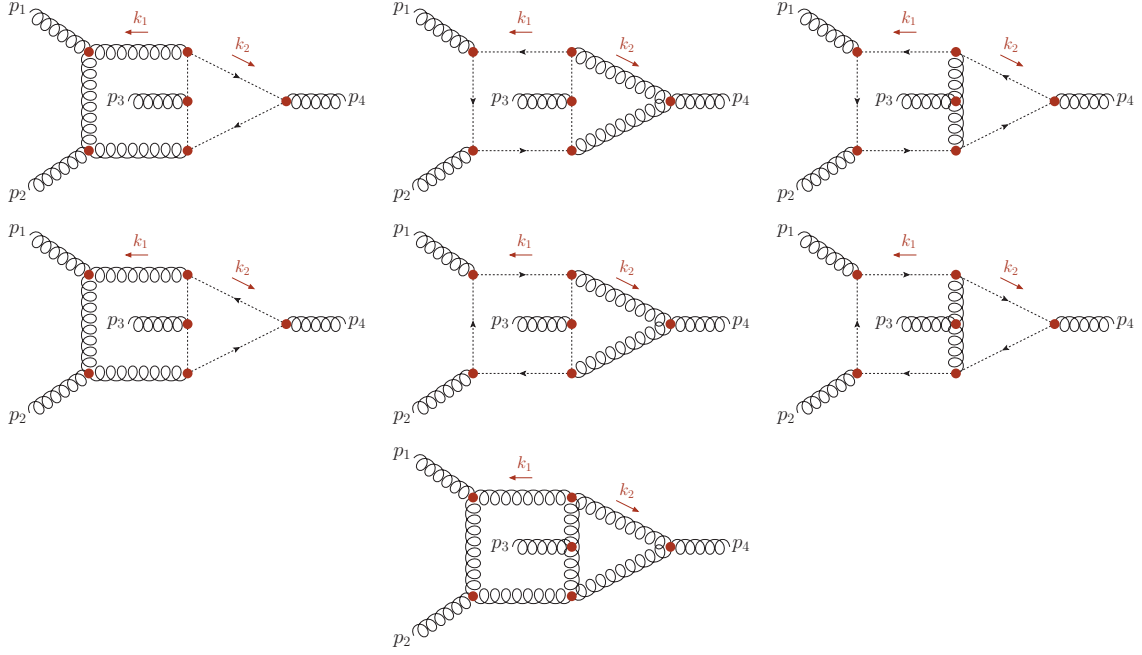


Figure 4: Feynman graphs contributing to the non-planar double-box numerator under study. There are four contributions, considering gluons and (anti-)ghosts running within the loops.

describing this topology coincide with the ones of penta-triangle topology, but only the first six of those propagators appear in the denominator, with the first one being repeated and thus being raised to the second power. The analysis, projecting over 6 or 9 propagators, works for all cases, as in the double-box, in both $d = 4 - 2\epsilon$ and $d = 4$ dimensions. Of course, in the final expression of Eq. (2.6), integrals with a doubled propagator occur, which in any case have to be evaluated in all cases by IBP identities, or otherwise, independently from the integrand-level reduction discussed in this paper.

3.1.4 Non-planar double box topologies

Here we focus on the numerator of the non-planar double-box topology constructed by the seven Feynman graphs drawn in Fig. 4. The depicted graphs are part of the full-color scattering amplitude of the process $gg \rightarrow gg$. The inverse propagators describing the family of this topology are chosen as

$$D_1 = k_1^2, \quad D_2 = (k_1 + p_1)^2, \quad D_3 = (k_1 + p_{12})^2, \quad D_4 = (k_1 + k_2 - p_3)^2, \\ D_5 = (k_1 + k_2)^2, \quad D_6 = k_2^2, \quad D_7 = (k_2 - p_{123})^2, \quad D_8 = (k_2 - p_{12})^2, \quad D_9 = (k_2 - p_1)^2$$

We seek again to solve Eq. (2.18) using cut equations and the known analytic expression of the numerator. The top sector cut equations

$$D_1 = D_2 = D_3 = D_4 = D_5 = D_6 = D_7 = 0 \quad (3.19)$$

Level	Number of cuts	Number of coefficients	Scaling
7	1	97	5,4,4
6	7	812	4,4,4
5	21	1612	3,3,3
4	35	922	2,2,2
3	35	124	1,1,1
2	21	0	0,0,0

Table 6: Non-planar double box linear fit information beginning with 7 cut.

result in the determination of 7 invariants

$$\begin{aligned}
k_1 \cdot k_1 \rightarrow 0, \quad k_1 \cdot k_2 \rightarrow 0, \quad k_1 \cdot p_1 \rightarrow 0, \quad k_1 \cdot p_2 \rightarrow -\frac{s}{2}, \\
k_2 \cdot k_2 \rightarrow 0, \quad k_2 \cdot p_2 \rightarrow k_1 \cdot p_3 - k_2 \cdot p_1, \quad k_2 \cdot p_3 \rightarrow -(k_1 \cdot p_3)
\end{aligned} \tag{3.20}$$

By applying the above relation on both sides of Eq. (2.18) we can fully determine the polynomial P_7 . The polynomial P_7 consists of 97 coefficients over the ISP monomials $\{k_1 \cdot p_3, k_1 \cdot \eta, k_2 \cdot p_1, k_2 \cdot \eta\}$.

Subtracting the P_7 in Eq. (2.18), we can now determine the polynomials P_6 in the same way. There are seven six-cuts and therefore seven P_6 polynomials to determine. As an example, the first six-cut,

$$D_2 = D_3 = D_4 = D_5 = D_6 = D_7 = 0 \tag{3.21}$$

leads to

$$\begin{aligned}
k_1 \cdot p_2 \rightarrow -\frac{s}{2}, \quad k_2 \cdot p_3 \rightarrow -(k_2 \cdot p_1) - k_2 \cdot p_2, \quad k_1 \cdot p_3 \rightarrow k_2 \cdot p_1 + k_2 \cdot p_2, \\
k_1 \cdot k_2 \rightarrow k_1 \cdot p_1, \quad k_1 \cdot k_1 \rightarrow -2k_1 \cdot p_1, \quad k_2 \cdot k_2 \rightarrow 0
\end{aligned} \tag{3.22}$$

whereas there are now 5 ISP $\{k_1 \cdot p_1, k_1 \cdot \eta, k_2 \cdot p_1, k_2 \cdot p_2, k_2 \cdot \eta\}$. The polynomial $P_1^{(6)}$ consists of 126 coefficients. The data for all cuts are summarized in Tab. 1. The analytic solutions for the polynomials satisfy explicitly Eq. (2.18).

We now seek to solve Eq. (2.19), namely projecting over all 9 propagators in the non-planar double-box topology. The top-level cut equations read

$$D_1 = D_2 = D_3 = D_4 = D_5 = D_6 = D_7 = D_8 = D_9 = 0 \tag{3.23}$$

which leads to

$$\begin{aligned}
k_1 \cdot k_1 \rightarrow 0, \quad k_1 \cdot k_2 \rightarrow 0, \quad k_1 \cdot p_1 \rightarrow 0, \quad k_1 \cdot p_2 \rightarrow -\frac{s}{2}, \quad k_1 \cdot p_3 \rightarrow \frac{s}{2}, \\
k_2 \cdot k_2 \rightarrow 0, \quad k_2 \cdot p_1 \rightarrow 0, \quad k_2 \cdot p_2 \rightarrow \frac{s}{2}, \quad k_2 \cdot p_3 \rightarrow -\frac{s}{2}
\end{aligned} \tag{3.24}$$

By applying the above relation on both sides of Eq. (2.19), we can fully determine the polynomial P_9 . The polynomial P_9 consists of 15 coefficients over the ISP monomials $\{k_1 \cdot \eta, k_2 \cdot \eta\}$.

Level	Number of cuts	Number of coefficients	Scaling
9	1	15	4,4,4
8	9	267	4,4,4
7	36	1168	3,3,3
6	84	1601	2,2,2
5	126	700	1,1,1
4	126	72	0,0,0

Table 7: Penta-triangle linear fit information beginning with 9-cut.

Subtracting as before the P_9 in Eq. (2.19), we can now determine the polynomials P_8 in the same way. There are nine 8-cuts and therefore nine P_8 polynomials to determine. As an example, the first 8-cut,

$$D_2 = D_3 = D_4 = D_5 = D_6 = D_7 = D_8 = D_9 = 0 \quad (3.25)$$

leads to

$$\begin{aligned} k_2 \cdot p_1 \rightarrow 0, \quad k_2 \cdot p_2 \rightarrow \frac{s}{2}, \quad k_1 \cdot p_2 \rightarrow -\frac{s}{2}, \quad k_2 \cdot p_3 \rightarrow -\frac{s}{2}, \quad k_1 \cdot p_3 \rightarrow \frac{s}{2}, \\ k_1 \cdot k_2 \rightarrow k_1 \cdot p_1, \quad k_1 \cdot k_1 \rightarrow -2k_1 \cdot p_1, \quad k_2 \cdot k_2 \rightarrow 0 \end{aligned} \quad (3.26)$$

whereas there are now 3 ISP $\{k_1 \cdot p_1, k_1 \cdot \eta, k_2 \cdot \eta\}$. The polynomial $P_1^{(8)}$ consists of 35 coefficients. The data for all cuts are summarized in Tab. 7. The analytic solutions for the polynomials satisfy explicitly Eq. (2.19). The rest of the analysis, regarding the fit by cut and the global fit in $d = 4 - 2\epsilon$ and $d = 4$ dimensions, is the same as for the planar double box.

3.1.5 $gg \rightarrow t\bar{t}$

In this subsection, we tackle a numerator topology consisting of one massive propagator. More specifically, we study the topology consisting of the three Feynman graphs sketched in Fig. 5, which contribute to the two-loop scattering amplitude of $t\bar{t}$ production. Notice that in order to avoid unnecessary complications due to the appearance of four-dimensional spinors in the helicity amplitude at this stage of the investigation, the analytic expression of the numerator is constructed as fully summed over polarizations of the product of the two-loop contributions with the tree-order one, $\sum(\mathcal{M}^{(0)})^* \mathcal{M}^{(2)}$. The propagators describing the family of this topology are chosen as

$$\begin{aligned} D_1 = k_1^2, \quad D_2 = (k_1 + p_1)^2, \quad D_3 = (k_1 + p_{12})^2, \quad D_4 = (k_1 + k_2)^2, \quad D_5 = k_2^2, \\ D_6 = (k_2 - p_{123})^2 - m_t^2, \quad D_7 = (k_2 - p_{12})^2, \quad D_8 = (k_2 - p_1)^2, \quad D_9 = (k_1 + p_{123})^2 \end{aligned}$$

The 7-cut is given by

$$\begin{aligned} k_1 \cdot k_1 \rightarrow 0, \quad k_1 \cdot k_2 \rightarrow 0, \quad k_1 \cdot p_1 \rightarrow 0, \quad k_1 \cdot p_2 \rightarrow -\frac{s}{2}, \quad k_2 \cdot k_2 \rightarrow 0, \\ k_2 \cdot p_2 \rightarrow \frac{s}{2} - k_2 \cdot p_1, \quad k_2 \cdot p_3 \rightarrow -\frac{s}{2} \end{aligned} \quad (3.27)$$

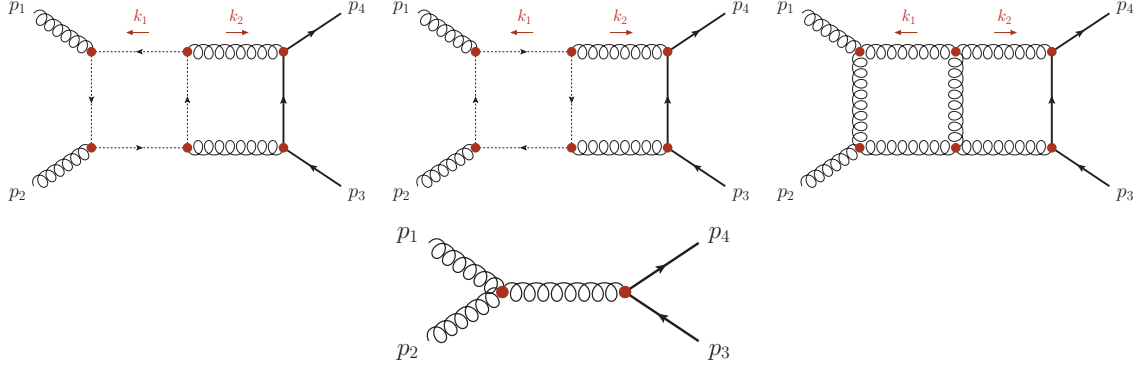


Figure 5: Feynman graphs contributing to the $gg \rightarrow t\bar{t}$ numerator under study. There are three contributions, considering gluons and (anti-)ghosts running within the k_1 loop, which are collected in the first line of this Figure. In the second line, we quote the tree-order graph used for the summation over polarizations. The thick black line indicates the (anti-)top quark.

Level	Number of cuts	Number of coefficients	Scaling
7	1	1	0,0,0
6	7	80	3,3,3
5	21	192	2,2,2
4	35	132	1,1,1
3	35	18	0,0,0
2	21	0	0,0,0

Table 8: $gg \rightarrow t\bar{t}$ linear fit information beginning with 7-cut.

and in that case the P_7 polynomial has no dependence on the loop momenta, $P_7 = 32s^3m_t^2(2m_t^2 - s - 2t)$. The first 6-cut is given by

$$\begin{aligned}
k_2 \cdot p_3 &\rightarrow -\frac{s}{2}, & k_2 \cdot p_1 &\rightarrow \frac{s}{2} - k_2 \cdot p_2, & k_1 \cdot p_2 &\rightarrow -\frac{s}{2}, \\
k_1 \cdot k_2 &\rightarrow k_1 \cdot p_1, & k_2 \cdot k_2 &\rightarrow 0, & k_1 \cdot k_1 &\rightarrow -2k_1 \cdot p_1
\end{aligned}
\tag{3.28}$$

and the corresponding P_6 polynomials consists of 15 monomials over $\{k_1 \cdot p_1, k_1 \cdot p_3, k_2 \cdot p_2\}$. The data for all cuts are summarized in Tab. 8. The analytic solutions for the polynomials satisfy explicitly Eq. (2.18). As is evident, for processes involving quarks, even massive, the reduction is an order of magnitude simpler than in the case of fully gluonic amplitudes.

Projecting over all 9 propagators in this topology, the 9-cut is given by

$$\begin{aligned}
k_1 \cdot k_1 &\rightarrow 0, & k_1 \cdot k_2 &\rightarrow 0, & k_1 \cdot p_1 &\rightarrow 0, & k_1 \cdot p_2 &\rightarrow -\frac{s}{2}, & k_1 \cdot p_3 &\rightarrow \frac{s}{2}, \\
k_2 \cdot k_2 &\rightarrow 0, & k_2 \cdot p_1 &\rightarrow 0, & k_2 \cdot p_2 &\rightarrow \frac{s}{2}, & k_2 \cdot p_3 &\rightarrow -\frac{s}{2}
\end{aligned}
\tag{3.29}$$

with P_9 given as before by $P_9 = 32s^3m_t^2(2m_t^2 - s - 2t)$. The data for all cuts are summarized in Tab. 8. The analytic solutions for the polynomials satisfy explicitly Eq. (2.19).

Level	Number of cuts	Number of coefficients	Scaling
9	1	1	0,0,0
6	9	17	2,1,2
5	36	122	2,2,2
4	84	197	1,1,1
3	126	83	0,0,0
4	126	0	0,0,0

Table 9: $gg \rightarrow t\bar{t}$ linear fit information beginning with 9-cut.

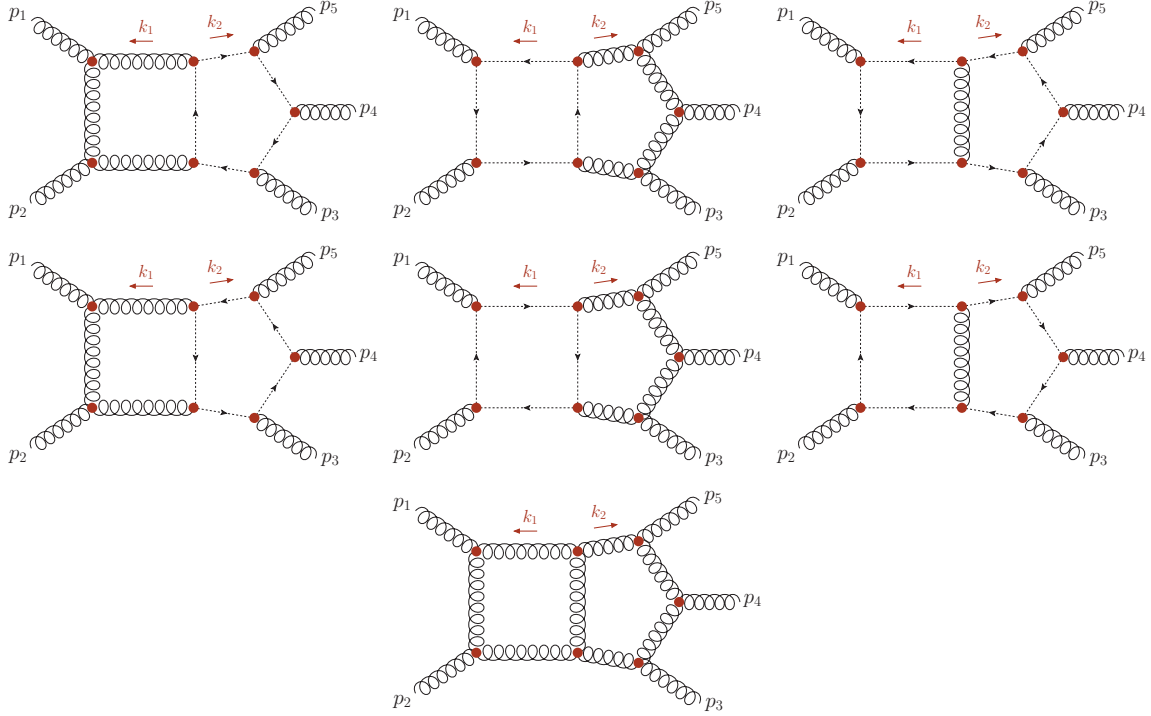


Figure 6: Feynman graphs contributing to the penta-box numerator under study. There are seven contributions, considering gluons and (anti-)ghosts running within the loops.

In both cases, the rest of the analysis works along the same lines as described for the double-box presented above.

3.2 Five-Point Kinematics

3.2.1 Penta-box topologies

Here we consider the numerator of the penta-box topology constructed by the seven Feynman graphs depicted in Fig. 6, which contributes to the scattering amplitude of the process $gg \rightarrow ggg$. For the analysis presented below, we have used the following helicity assignment: $\lambda_1 = +1, \lambda_2 = +1, \lambda_3 = -1, \lambda_4 = -1, \lambda_5 = -1$, for the helicities of the incoming gluons.

Our choice for the inverse propagators describing the family of this topology is the following

$$\begin{aligned} D_1 &= k_1^2, & D_2 &= (k_1 + p_1)^2, & D_3 &= (k_1 + p_{12})^2, & D_4 &= (k_1 + k_2)^2, \\ D_5 &= k_2^2, & D_6 &= (k_2 - p_{1234})^2, & D_7 &= (k_2 - p_{123})^2, & D_8 &= (k_2 - p_{12})^2, \\ D_9 &= (k_1 + p_{123})^2, & D_{10} &= (k_1 + p_{1234})^2, & D_{11} &= (k_2 - p_1)^2 \end{aligned} \quad (3.30)$$

The external kinematics is described by 4 independent momenta and five independent invariants, which can be chosen to be $S_5 = \{s_{12}, s_{23}, s_{34}, s_{45}, s_{15}\}$, where $s_{ij} = (p_i + p_j)^2$. In order to proceed with the reduction in an analytic setup, the expression of the numerator needs to be expressed in terms of the 11 invariants V_{11} , $k_i \cdot k_j$, with $i, j = 1, 2$, and $k_i \cdot p_j$ with $i = 1, 2, j = 1, \dots, 4$. Since the analytic expression of the numerator involves the polarization vectors of the external gluons, $\varepsilon_i, i = 1, \dots, 5$, scalar products of the form $k_i \cdot \varepsilon_j$ and $p_i \cdot \varepsilon_j$ need to be expressed in terms of the variables S_5 and V_{11} . To this end, the following relation is used

$$q_i \cdot q_j = G_{kl}^{-1} q_i \cdot p_k q_j \cdot p_l \quad (3.31)$$

where q_i stands for any momentum or polarization vector and G denotes the Gram matrix, $G_{ij} = p_i \cdot p_j, i, j = 1, \dots, 4$ expressed in terms of the S_5 variables. Barring that the analytic expression for the inverse Gram matrix and the numerator are complicated expressions, it is convenient to work in a numerical setup, using exact arithmetic. The numerical values for the variables S_5 , are chosen as $\{s_{12} \rightarrow 1, s_{34} \rightarrow \frac{1}{4}, s_{45} \rightarrow \frac{1}{4}, s_{15} \rightarrow -\frac{1}{4}, s_{23} \rightarrow -\frac{1}{8}\}$. The polarization vectors are defined by

$$\begin{aligned} \varepsilon_\mu^+(p_i) &= \frac{1}{\sqrt{2}\bar{u}_-(p_{i+1})u_+(p_i)} \bar{u}_-(p_{i+1})\gamma_\mu u_-(p_i) \\ \varepsilon_\mu^-(p_i) &= -\frac{1}{\sqrt{2}\bar{u}_+(p_{i+1})u_-(p_i)} \bar{u}_+(p_{i+1})\gamma_\mu u_-(p_i) \end{aligned} \quad (3.32)$$

for $i = 1, \dots, 5$, where in the above formula the following the $p_6 \rightarrow p_1$ identification is assumed. With the above identifications, the numerator consists of monomials composed of the V_{11} variables, with exact numerical coefficients.

We seek to solve Eq. (2.20). The maximal cut is given by

$$\begin{aligned} k_1 \cdot k_1 &\rightarrow 0, & k_1 \cdot k_2 &\rightarrow 0, & k_1 \cdot p_1 &\rightarrow 0, & k_1 \cdot p_2 &\rightarrow -\frac{s_{12}}{2}, & k_2 \cdot k_2 &\rightarrow 0, \\ k_2 \cdot p_2 &\rightarrow \frac{s_{12}}{2} - k_2 \cdot p_1, & k_2 \cdot p_3 &\rightarrow \frac{s_{45}}{2} - \frac{s_{12}}{2}, & k_2 \cdot p_4 &\rightarrow -\frac{s_{45}}{2} \end{aligned} \quad (3.33)$$

The P_8 polynomial consists of 50 terms, composed of monomials in the ISP variables $\{k_1 \cdot p_3, k_1 \cdot p_4, k_2 \cdot p_1\}$. By following the usual subtraction procedure, the solution for all polynomials is found to satisfy Eq. (2.20). The data of this solution are given in Tab. 10. Seeking now to solve Eq. (2.21) the maximal cut is given by

$$\begin{aligned} k_1 \cdot k_1 &\rightarrow 0, & k_1 \cdot k_2 &\rightarrow 0, & k_1 \cdot p_1 &\rightarrow 0, & k_1 \cdot p_2 &\rightarrow -\frac{s_{12}}{2}, & k_1 \cdot p_3 &\rightarrow \frac{s_{12}}{2} - \frac{s_{45}}{2}, \\ k_1 \cdot p_4 &\rightarrow \frac{s_{45}}{2}, & k_2 \cdot k_2 &\rightarrow 0, & k_2 \cdot p_1 &\rightarrow 0, & k_2 \cdot p_2 &\rightarrow \frac{s_{12}}{2}, \\ k_2 \cdot p_3 &\rightarrow \frac{s_{45}}{2} - \frac{s_{12}}{2}, & k_2 \cdot p_4 &\rightarrow -\frac{s_{45}}{2} \end{aligned} \quad (3.34)$$

Level	Number of cuts	Number of coefficients	Scaling
8	1	50	4,5,5
7	8	705	4,4,5
6	28	2550	4,4,4
5	56	3508	3,3,3
4	70	1902	2,2,2
3	56	348	1,1,1
2	28	12	0,0,0

Table 10: Penta-box linear fit information beginning with 8-cut.

Level	Number of cuts	Number of coefficients	Scaling
11	1	1	0,0,0
10	11	47	3,4,4
9	55	502	3,4,4
8	165	2313	3,3,3
7	330	3715	2,2,2
6	462	2255	1,1,1
5	462	425	0,0,0

Table 11: Penta-box linear fit information beginning with 11-cut.

and as before, the cut data are shown in Tab. 11. The fit by cut and the global fit in $d = 4 - 2\epsilon$ dimensions is realized as before through the numerical representation of the loop momenta given in section 2.2.

3.2.2 $t\bar{t}H$

Herein, we study a numerator topology consisting of two massive propagators. This corresponds to the three graphs depicted in Fig. 7, which contribute to the scattering amplitude of the process $gg \rightarrow t\bar{t}H$. We again note that in order to avoid unnecessary complications due to the appearance in the helicity amplitude of four-dimensional spinors, the analytic expression of the numerator is constructed as a fully summed over polarizations of the product of the two-loop contributions with the tree-order one. The inverse propagators describing the family for this topology are chosen as

$$\begin{aligned}
D_1 &= k_1^2, & D_2 &= (k_1 + p_1)^2, & D_3 &= (k_1 + p_{12})^2, & D_4 &= (k_1 + k_2)^2, & D_5 &= k_2^2, \\
D_6 &= (k_2 - p_{1234})^2 - m_t^2, & D_7 &= (k_2 - p_{123})^2 - m_t^2, & D_8 &= (k_2 - p_{12})^2, \\
D_9 &= (k_1 + p_{123})^2, & D_{10} &= (k_1 + p_{1234})^2, & D_{11} &= (k_2 - p_1)^2
\end{aligned} \tag{3.35}$$

The 8-cut is given by

$$\begin{aligned}
&k_1 \cdot k_1 \rightarrow 0, \quad k_1 \cdot k_2 \rightarrow 0, \quad k_1 \cdot p_1 \rightarrow 0, \quad k_1 \cdot p_2 \rightarrow -\frac{s_{12}}{2}, \quad k_2 \cdot k_2 \rightarrow 0, \\
&k_2 \cdot p_2 \rightarrow \frac{s_{12}}{2} - k_2 \cdot p_1, \quad k_2 \cdot p_3 \rightarrow \frac{1}{2}(-m_t^2 - s_{12} + s_{45}), \quad k_2 \cdot p_4 \rightarrow \frac{1}{2}(m_t^2 - s_{45})
\end{aligned} \tag{3.36}$$

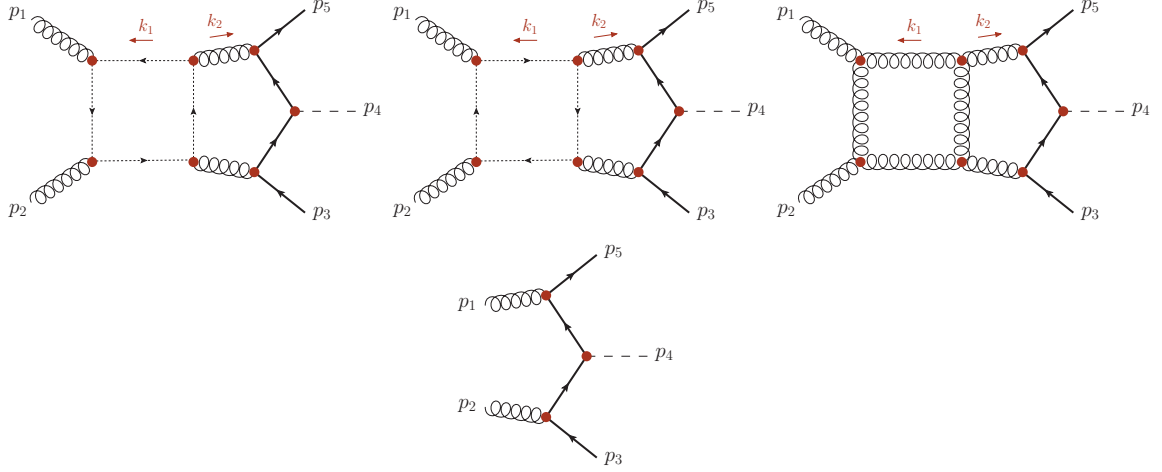


Figure 7: Feynman graphs contributing to the $gg \rightarrow t\bar{t}H$ numerator under study. There are three contributions, considering gluons and (anti-)ghosts running within the k_1 loop, which are collected in the first line of this Figure. In the second line, we quote the tree-order graph used for the summation over polarizations. The dashed line indicates the Higgs boson.

Level	Number of cuts	Number of coefficients	Scaling
8	1	32	4,3,5
7	8	293	4,3,4
6	28	735	3,2,2
5	56	651	2,2,2
4	70	181	1,1,1
3	56	8	0,0,0

Table 12: $gg \rightarrow t\bar{t}H$ linear fit information beginning with 8-cut.

and in that case, the P_8 polynomial consists of 32 terms composed of monomials in the ISP variables $k_1 \cdot p_3, k_1 \cdot p_4, k_2 \cdot p_1$. The data for all cuts are summarized in Tab. 12. The analytic solutions for the polynomials satisfy explicitly Eq. (2.18). Projecting over all 11 propagators in this topology, the 11-cut is given by

$$\begin{aligned}
k_1 \cdot k_1 &\rightarrow 0, & k_1 \cdot k_2 &\rightarrow 0, & k_1 \cdot p_1 &\rightarrow 0, & k_1 \cdot p_2 &\rightarrow -\frac{s_{12}}{2}, & k_1 \cdot p_3 &\rightarrow \frac{1}{2}(s_{12} - s_{45}), \\
k_1 \cdot p_4 &\rightarrow \frac{1}{2}(s_{45} - m_t^2), & k_2 \cdot k_2 &\rightarrow 0, & k_2 \cdot p_1 &\rightarrow 0, & k_2 \cdot p_2 &\rightarrow \frac{s_{12}}{2}, \\
k_2 \cdot p_3 &\rightarrow \frac{1}{2}(-m_t^2 - s_{12} + s_{45}), & k_2 \cdot p_4 &\rightarrow \frac{1}{2}(m_t^2 - s_{45})
\end{aligned} \tag{3.37}$$

with P_{11} consisting of a single term expressed as a function of the external invariants $\{m_H, m_t, s_{12}, s_{15}, s_{23}, s_{34}, s_{45}\}$. The data for all cuts are summarized in Tab. 13. The analytic solutions for the polynomials satisfy explicitly Eq. (2.19). In both cases, the rest of the analysis works in the same lines as for the double-box presented above.

Level	Number of cuts	Number of coefficients	Scaling
11	1	1	0,0,0
10	11	32	2,2,2
9	55	270	2,2,3
8	165	766	2,2,2
7	330	734	1,1,1
6	462	158	0,0,0

Table 13: $gg \rightarrow t\bar{t}H$ linear fit information beginning with 8-cut.

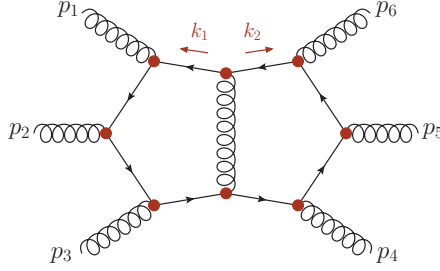


Figure 8: Feynman graph contributing to the six-gluon numerator under study. The normal line is used for denoting a massless quark.

3.3 Six-Point Kinematics

3.3.1 Six-gluon topology

In this subsection, we apply our method to the case of the six-gluon two-loop numerator topology of Fig. 8. This graph is part of the $gg \rightarrow gggg$ scattering amplitude. For the analysis presented below, we have used the following helicity assignment: $\lambda_1 = +1, \lambda_2 = +1, \lambda_3 = -1, \lambda_4 = -1, \lambda_5 = -1, \lambda_6 = -1$, for the helicities of the incoming gluons. We define the propagators of the family in which this topology belongs, as

$$\begin{aligned}
D_1 &= k_1^2, & D_2 &= (k_1 + p_1)^2, & D_3 &= (k_1 + p_{12})^2, & D_4 &= (k_1 + p_{123})^2, & D_5 &= (k_1 + k_2)^2, \\
D_6 &= k_2^2, & D_7 &= (k_2 - p_{12345})^2, & D_8 &= (k_2 - p_{1234})^2, & D_9 &= (k_2 - p_{123})^2, \\
D_{10} &= (k_1 + p_{1234})^2, & D_{11} &= (k_1 + p_{12345})^2, & D_{12} &= (k_2 - p_{12})^2, & D_{13} &= (k_2 - p_1)^2
\end{aligned}$$

Since out of the six external momenta only four are independent in $d = 4$ dimensions, not all 13 propagators in Eq. (3.3.1) are independent. In general, for any n -point amplitude, with $n \geq 5$, only 11 propagators are independent. We have chosen the following subset, $\{D_1, \dots, D_{10}, D_{13}\}$ having expressed p_5 in terms of p_1, \dots, p_4 through Eq. (3.31). As in the case of the penta-box, section 3.2.1, the analytic expressions are hardly manageable, and it is convenient to work in a numerical setup, using exact arithmetic. The numerical values

Level	Number of cuts	Number of coefficients	Scaling
9	1	1	4,4,6
8	9	355	4,4,6
7	36	1949	4,4,5
6	84	4462	4,4,4
5	126	4540	3,3,3
4	126	2016	2,2,2
3	84	334	1,1,1
2	36	16	0,0,0

Table 14: 6 gluon linear fit information beginning with 9-cut.

of the invariants are chosen as ⁷

$$\left\{ s_{12} \rightarrow 4, s_{23} \rightarrow -1, s_{34} \rightarrow 1, s_{45} \rightarrow \frac{5}{4}, s_{56} \rightarrow \frac{1}{2}, s_{16} \rightarrow -1, s_{123} \rightarrow 2, s_{234} \rightarrow -1, s_{345} \rightarrow \frac{31}{12} \right\},$$

with $s_{ijk} = (p_i + p_j + p_k)^2$. For the polarization vectors we follow Eq. (3.32), with the identification of $p_7 \rightarrow p_1$. The 9-cut

$$D_1 = \dots = D_9 = 0 \quad (3.38)$$

is given, in the numerical point chosen, by

$$\begin{aligned} k_1 \cdot k_1 \rightarrow 0, \quad k_1 \cdot k_2 \rightarrow 0, \quad k_1 \cdot p_1 \rightarrow 0, \quad k_1 \cdot p_2 \rightarrow -2, \quad k_1 \cdot p_3 \rightarrow 1, \quad k_2 \cdot k_2 \rightarrow 0, \\ k_2 \cdot p_2 \rightarrow \frac{5}{2} - \frac{5k_2 \cdot p_1}{3}, \quad k_2 \cdot p_3 \rightarrow \frac{2k_2 \cdot p_1}{3} - \frac{3}{2}, \quad k_2 \cdot p_4 \rightarrow -\frac{3}{4} \end{aligned} \quad (3.39)$$

The reduction data are given in Tab. 14. Projecting over the set of 11 propagators, referred above, the 11-cut is given by

$$\begin{aligned} k_1 \cdot k_1 \rightarrow 0, \quad k_1 \cdot k_2 \rightarrow 0, \quad k_1 \cdot p_1 \rightarrow 0, \quad k_1 \cdot p_2 \rightarrow -2, \quad k_1 \cdot p_3 \rightarrow 1, \\ k_1 \cdot p_4 \rightarrow \frac{3}{4}, \quad k_2 \cdot k_2 \rightarrow 0, \quad k_2 \cdot p_1 \rightarrow 0, \quad k_2 \cdot p_2 \rightarrow \frac{5}{2}, \\ k_2 \cdot p_3 \rightarrow -\frac{3}{2}, \quad k_2 \cdot p_4 \rightarrow -\frac{3}{4} \end{aligned} \quad (3.40)$$

and the reduction data are summarized in Tab. 15

4 Summary and Discussion

In this paper, we have studied the integrand-level reduction at two loops, solving Eq. (2.4) and Eq. (2.17). Let us briefly summarize our findings:

⁷Notice that for 4-dimensional external momenta only 8 invariants are independent. In fact, s_{345} , for instance, can be determined by the requirement that the five-momenta Gram determinant, $G(12345)$, vanishes, see also ref. [104].

Level	Number of cuts	Number of coefficients	Scaling
11	1	1	0,0,0
10	11	41	3,3,3
9	55	505	3,3,5
8	165	2365	3,3,4
7	330	4780	3,3,3
6	462	4290	2,2,2
5	462	1592	1,1,1
4	330	200	0,0,0

Table 15: 6 gluon linear fit information beginning with 11-cut.

- We solved the reduction equation by two generic methods, namely, fit by cut and global fit. In the fit by cut approach, we constructed the solutions to the cut equations Eq. (2.8) and then used them to fit the polynomials P appearing in Eq. (2.4).
- A novel element of our studies is the observation that the reduction equation can be extended to include all inverse propagators characterizing a given family and not just the ones appearing in the Feynman graphs under consideration, see Eq. (2.17). This way, the polynomials depend on a smaller number of variables. Moreover, this approach allows us to use the solutions of the cut equations for all Feynman graphs under the same family.
- We applied our method in both $d = 4 - 2\epsilon$ and $d = 4$ dimensions. In the $d = 4 - 2\epsilon$ case, the numerator is expressed as a function of the four-dimensional external momenta and polarization vectors and the four-dimensional part of the loop momenta along with the μ_{ij} terms. In all cases, this is readily possible, since the numerator has been known analytically. Cut equations admit a unique solution in terms of the ISP and can be used to fit the coefficients of the polynomials either analytically or numerically.
- In $d = 4$ dimensions, the cut equations do not admit, in general, a unique solution in terms of ISP. We showed, nevertheless, how to construct solutions to both Eq. (2.4) and Eq. (2.17).
- In the global fit approach, both in $d = 4 - 2\epsilon$ and $d = 4$ dimensions, solutions to the cut equations are not necessary, but determining the coefficients of the polynomials involves solving linear equations with relatively large matrices. It is though a plausible alternative to the fit by cut approach, especially in validating Eq. (2.4) and Eq. (2.17).
- We have successfully studied the reduction equations for several cases in 4-, 5- and 6-particle topologies, with massless and massive external particles and internal propagators: double-box, penta-triangle, hexa-bubble, non-planar double-box, $t\bar{t}$, penta-box, $t\bar{t}H$ and 6-gluon with a closed quark loop. We conclude that two-loop reduction at the integrand level is within reach for arbitrary processes. We plan to

implement the solutions of the cut equations in a numerical setup [80], in order to allow for a fully-fledged numerical reduction of two-loop integrand numerators.

A crucial element in the direction of the construction of a generic automated two-loop amplitude computational framework based on the integrand-level reduction is the calculation of the dimensionally regulated amplitudes. As we have seen in this paper, the numerical evaluation of the integrands needs to address the dependence on μ_{ij} and ϵ terms. This issue is currently under investigation [93], and we plan to publish our results in the near future [105].

In order to provide useful results for phenomenological applications, the two-loop Feynman integrals in Eq. (2.6) need to be provided. At this time, a fully numerical computation of all two-loop integrals [68, 76] seems quite challenging. Analytic results, on the other hand, are available for master integrals in more and more cases over the recent years [104, 106–123], but IBP solutions in expressing Feynman integrals in terms of master integrals are necessary as well. In principle, this can be achieved in a process-independent way by providing appropriate IBP tables that express the Feynman integrals of Eq. (2.7) in terms of currently known MIs. We plan to provide a proof of concept of a complete computational framework in the near future [124], combining HELAC-2LOOP amplitude generator for the numerical evaluation of the numerators in $d = 4 - 2\epsilon$ dimensions, the numerical implementation of the reduction equation, Eq. (2.17), and the interface to evaluating the currently known Feynman integrals appearing in Eq. (2.6), including a detailed analysis of numerical accuracy and performance, paving the way to automated two-loop calculations.

Acknowledgments

We thank Simon Badger, Hjalte Frellesvig, Adam Kardos, Tiziano Peraro, Vasily Sotnikov, and Yang Zhang for useful discussions. The work of G. Bevilacqua, C. G. Papadopoulos, and A. Spourdalakis is supported by the Hellenic Foundation for Research and Innovation (H.F.R.I.) under the "2nd Call for H.F.R.I. Research Projects to support Faculty Members & Researchers" (Project Number: 02674 HOCTools-II). The work of D. Canko is supported by the European Research Council (ERC) under the European Union's Horizon Europe research and innovation program grant agreement 101040760, *High-precision multi-leg Higgs and top physics with finite fields* (ERC Starting Grant FFHiggsTop). C. G. Papadopoulos would like to thank the Department of Theoretical Physics at CERN and the Aspen Center for Physics and the Simons Foundation, for their kind hospitality.

References

- [1] A. Dainese, M. Mangano, A. B. Meyer, A. Nisati, G. Salam, and M. A. Vesterinen, eds., *Report on the Physics at the HL-LHC, and Perspectives for the HE-LHC*, vol. 7/2019 of *CERN Yellow Reports: Monographs*. CERN, Geneva, Switzerland, 2019.
- [2] F. Caola, W. Chen, C. Duhr, X. Liu, B. Mistlberger, F. Petriello, G. Vita, and S. Weinzierl, *The Path forward to N^3 LO*, in *Snowmass 2021*, 3, 2022. [arXiv:2203.06730](https://arxiv.org/abs/2203.06730).

- [3] CMS Collaboration, *Highlights of the HL-LHC physics projections by ATLAS and CMS*, [arXiv:2504.00672](#).
- [4] FCC Collaboration, M. Benedikt et al., *Future Circular Collider Feasibility Study Report: Volume 1, Physics, Experiments, Detectors*, [arXiv:2505.00272](#).
- [5] A. Huss, J. Huston, S. Jones, M. Pellen, and R. Röntsch, *Les Houches 2023 – Physics at TeV Colliders: Report on the Standard Model Precision Wishlist*, [arXiv:2504.06689](#).
- [6] S. Badger, C. Brønnum-Hansen, H. B. Hartanto, and T. Peraro, *First look at two-loop five-gluon scattering in QCD*, *Phys. Rev. Lett.* **120** (2018), no. 9 092001, [[arXiv:1712.02229](#)].
- [7] S. Badger, C. Brønnum-Hansen, H. B. Hartanto, and T. Peraro, *Analytic helicity amplitudes for two-loop five-gluon scattering: the single-minus case*, *JHEP* **01** (2019) 186, [[arXiv:1811.11699](#)].
- [8] S. Abreu, F. Febres Cordero, H. Ita, B. Page, and V. Sotnikov, *Planar Two-Loop Five-Parton Amplitudes from Numerical Unitarity*, *JHEP* **11** (2018) 116, [[arXiv:1809.09067](#)].
- [9] S. Abreu, J. Dormans, F. Febres Cordero, H. Ita, and B. Page, *Analytic Form of Planar Two-Loop Five-Gluon Scattering Amplitudes in QCD*, *Phys. Rev. Lett.* **122** (2019), no. 8 082002, [[arXiv:1812.04586](#)].
- [10] S. Abreu, J. Dormans, F. Febres Cordero, H. Ita, B. Page, and V. Sotnikov, *Analytic Form of the Planar Two-Loop Five-Parton Scattering Amplitudes in QCD*, *JHEP* **05** (2019) 084, [[arXiv:1904.00945](#)].
- [11] S. Badger, D. Chicherin, T. Gehrmann, G. Heinrich, J. M. Henn, T. Peraro, P. Wasser, Y. Zhang, and S. Zoia, *Analytic form of the full two-loop five-gluon all-plus helicity amplitude*, *Phys. Rev. Lett.* **123** (2019), no. 7 071601, [[arXiv:1905.03733](#)].
- [12] H. B. Hartanto, S. Badger, C. Brønnum-Hansen, and T. Peraro, *A numerical evaluation of planar two-loop helicity amplitudes for a W-boson plus four partons*, *JHEP* **09** (2019) 119, [[arXiv:1906.11862](#)].
- [13] H. A. Chawdhry, M. Czakon, A. Mitov, and R. Poncelet, *Two-loop leading-color helicity amplitudes for three-photon production at the LHC*, *JHEP* **06** (2021) 150, [[arXiv:2012.13553](#)].
- [14] S. Kallweit, V. Sotnikov, and M. Wiesemann, *Triphoton production at hadron colliders in NNLO QCD*, *Phys. Lett. B* **812** (2021) 136013, [[arXiv:2010.04681](#)].
- [15] S. Abreu, F. Febres Cordero, H. Ita, B. Page, and V. Sotnikov, *Leading-color two-loop QCD corrections for three-jet production at hadron colliders*, *JHEP* **07** (2021) 095, [[arXiv:2102.13609](#)].
- [16] S. Badger, H. B. Hartanto, and S. Zoia, *Two-Loop QCD Corrections to $Wb\bar{b}$ Production at Hadron Colliders*, *Phys. Rev. Lett.* **127** (2021), no. 1 012001, [[arXiv:2102.02516](#)].
- [17] S. Badger, C. Brønnum-Hansen, D. Chicherin, T. Gehrmann, H. B. Hartanto, J. Henn, M. Marcoli, R. Moodie, T. Peraro, and S. Zoia, *Virtual QCD corrections to gluon-initiated diphoton plus jet production at hadron colliders*, *JHEP* **11** (2021) 083, [[arXiv:2106.08664](#)].
- [18] S. Badger, H. B. Hartanto, J. Kryś, and S. Zoia, *Two-loop leading-colour QCD helicity amplitudes for Higgs boson production in association with a bottom-quark pair at the LHC*, *JHEP* **11** (2021) 012, [[arXiv:2107.14733](#)].

- [19] H. A. Chawdhry, M. Czakon, A. Mitov, and R. Poncelet, *Two-loop leading-colour QCD helicity amplitudes for two-photon plus jet production at the LHC*, *JHEP* **07** (2021) 164, [[arXiv:2103.04319](#)].
- [20] H. A. Chawdhry, M. Czakon, A. Mitov, and R. Poncelet, *NNLO QCD corrections to diphoton production with an additional jet at the LHC*, *JHEP* **09** (2021) 093, [[arXiv:2105.06940](#)].
- [21] M. Czakon, A. Mitov, and R. Poncelet, *Next-to-Next-to-Leading Order Study of Three-Jet Production at the LHC*, *Phys. Rev. Lett.* **127** (2021), no. 15 152001, [[arXiv:2106.05331](#)]. [Erratum: *Phys.Rev.Lett.* 129, 119901 (2022)].
- [22] S. Abreu, F. Febres Cordero, H. Ita, M. Klinkert, B. Page, and V. Sotnikov, *Leading-color two-loop amplitudes for four partons and a W boson in QCD*, *JHEP* **04** (2022) 042, [[arXiv:2110.07541](#)].
- [23] S. Badger, H. B. Hartanto, J. Kryś, and S. Zoia, *Two-loop leading colour helicity amplitudes for $W\gamma + j$ production at the LHC*, *JHEP* **05** (2022) 035, [[arXiv:2201.04075](#)].
- [24] S. Badger, M. Czakon, H. B. Hartanto, R. Moodie, T. Peraro, R. Poncelet, and S. Zoia, *Isolated photon production in association with a jet pair through next-to-next-to-leading order in QCD*, *JHEP* **10** (2023) 071, [[arXiv:2304.06682](#)].
- [25] S. Abreu, G. De Laurentis, H. Ita, M. Klinkert, B. Page, and V. Sotnikov, *Two-loop QCD corrections for three-photon production at hadron colliders*, *SciPost Phys.* **15** (2023), no. 4 157, [[arXiv:2305.17056](#)].
- [26] B. Agarwal, F. Buccioni, F. Devoto, G. Gambuti, A. von Manteuffel, and L. Tancredi, *Five-parton scattering in QCD at two loops*, *Phys. Rev. D* **109** (2024), no. 9 094025, [[arXiv:2311.09870](#)].
- [27] G. De Laurentis, H. Ita, M. Klinkert, and V. Sotnikov, *Double-virtual NNLO QCD corrections for five-parton scattering. I. The gluon channel*, *Phys. Rev. D* **109** (2024), no. 9 094023, [[arXiv:2311.10086](#)].
- [28] G. De Laurentis, H. Ita, and V. Sotnikov, *Double-virtual NNLO QCD corrections for five-parton scattering. II. The quark channels*, *Phys. Rev. D* **109** (2024), no. 9 094024, [[arXiv:2311.18752](#)].
- [29] S. Badger, H. B. Hartanto, Z. Wu, Y. Zhang, and S. Zoia, *Two-loop amplitudes for $\mathcal{O}(\alpha_s^2)$ corrections to $W\gamma\gamma$ production at the LHC*, *JHEP* **12** (2025) 221, [[arXiv:2409.08146](#)].
- [30] S. Badger, H. B. Hartanto, R. Poncelet, Z. Wu, Y. Zhang, and S. Zoia, *Full-colour double-virtual amplitudes for associated production of a Higgs boson with a bottom-quark pair at the LHC*, *JHEP* **03** (2025) 066, [[arXiv:2412.06519](#)].
- [31] J. Mazzitelli, V. Sotnikov, and M. Wiesemann, *Next-to-next-to-leading order event generation for Z-boson production in association with a bottom-quark pair*, [[arXiv:2404.08598](#)].
- [32] S. Badger, M. Becchetti, C. Brancaccio, H. B. Hartanto, and S. Zoia, *Numerical evaluation of two-loop QCD helicity amplitudes for $gg \rightarrow t\bar{t}g$ at leading colour*, *JHEP* **03** (2025) 070, [[arXiv:2412.13876](#)].
- [33] B. Agarwal, G. Heinrich, S. P. Jones, M. Kerner, S. Y. Klein, J. Lang, V. Magerya, and A. Olsson, *Two-loop amplitudes for $t\bar{t}H$ production: the quark-initiated N_f -part*, *JHEP* **05** (2024) 013, [[arXiv:2402.03301](#)]. [Erratum: *JHEP* 06, 142 (2024)].

- [34] G. De Laurentis, H. Ita, B. Page, and V. Sotnikov, *Compact Two-Loop QCD Corrections for Vjj Production in Proton Collisions*, [arXiv:2503.10595](#).
- [35] T. Hahn, *Generating Feynman diagrams and amplitudes with FeynArts 3*, *Comput. Phys. Commun.* **140** (2001) 418–431, [[hep-ph/0012260](#)].
- [36] P. Nogueira, *Automatic Feynman Graph Generation*, *J. Comput. Phys.* **105** (1993) 279–289.
- [37] S. Pozzorini, N. Schär, and M. F. Zoller, *Two-loop tensor integral coefficients in OpenLoops*, *JHEP* **05** (2022) 161, [[arXiv:2201.11615](#)].
- [38] D. Canko, G. Bevilacqua, and C. Papadopoulos, *Two-Loop Amplitude Reduction with HELAC*, *PoS RADCOR2023* (2024) 081, [[arXiv:2309.14886](#)].
- [39] T. Peraro and L. Tancredi, *Physical projectors for multi-leg helicity amplitudes*, *JHEP* **07** (2019) 114, [[arXiv:1906.03298](#)].
- [40] T. Peraro and L. Tancredi, *Tensor decomposition for bosonic and fermionic scattering amplitudes*, *Phys. Rev. D* **103** (2021), no. 5 054042, [[arXiv:2012.00820](#)].
- [41] C. Anastasiou, J. Karlen, and M. Vicini, *Tensor reduction of loop integrals*, *JHEP* **12** (2023) 169, [[arXiv:2308.14701](#)].
- [42] J. Goode, F. Herzog, A. Kennedy, S. Teale, and J. Vermaseren, *Tensor reduction for Feynman integrals with Lorentz and spinor indices*, *JHEP* **11** (2024) 123, [[arXiv:2408.05137](#)].
- [43] J. Goode, F. Herzog, and S. Teale, *OPITeR: A program for tensor reduction of multi-loop Feynman integrals*, *Comput. Phys. Commun.* **312** (2025) 109606, [[arXiv:2411.02233](#)].
- [44] D. A. Kosower and K. J. Larsen, *Maximal Unitarity at Two Loops*, *Phys. Rev. D* **85** (2012) 045017, [[arXiv:1108.1180](#)].
- [45] P. Mastrolia and G. Ossola, *On the Integrand-Reduction Method for Two-Loop Scattering Amplitudes*, *JHEP* **11** (2011) 014, [[arXiv:1107.6041](#)].
- [46] Y. Zhang, *Integrand-Level Reduction of Loop Amplitudes by Computational Algebraic Geometry Methods*, *JHEP* **09** (2012) 042, [[arXiv:1205.5707](#)].
- [47] S. Badger, H. Frellesvig, and Y. Zhang, *Hepta-Cuts of Two-Loop Scattering Amplitudes*, *JHEP* **04** (2012) 055, [[arXiv:1202.2019](#)].
- [48] P. Mastrolia, E. Mirabella, G. Ossola, and T. Peraro, *Scattering Amplitudes from Multivariate Polynomial Division*, *Phys. Lett. B* **718** (2012) 173–177, [[arXiv:1205.7087](#)].
- [49] P. Mastrolia, E. Mirabella, G. Ossola, and T. Peraro, *Integrand-Reduction for Two-Loop Scattering Amplitudes through Multivariate Polynomial Division*, *Phys. Rev. D* **87** (2013), no. 8 085026, [[arXiv:1209.4319](#)].
- [50] R. H. P. Kleiss, I. Malamos, C. G. Papadopoulos, and R. Verheyen, *Counting to One: Reducibility of One- and Two-Loop Amplitudes at the Integrand Level*, *JHEP* **12** (2012) 038, [[arXiv:1206.4180](#)].
- [51] P. Mastrolia, E. Mirabella, G. Ossola, and T. Peraro, *Multiloop Integrand Reduction for Dimensionally Regulated Amplitudes*, *Phys. Lett. B* **727** (2013) 532–535, [[arXiv:1307.5832](#)].
- [52] S. Badger, H. Frellesvig, and Y. Zhang, *A Two-Loop Five-Gluon Helicity Amplitude in QCD*, *JHEP* **12** (2013) 045, [[arXiv:1310.1051](#)].

- [53] H. Ita, *Two-loop Integrand Decomposition into Master Integrals and Surface Terms*, *Phys. Rev. D* **94** (2016), no. 11 116015, [[arXiv:1510.05626](#)].
- [54] P. Mastrolia, T. Peraro, and A. Primo, *Adaptive Integrand Decomposition in parallel and orthogonal space*, *JHEP* **08** (2016) 164, [[arXiv:1605.03157](#)].
- [55] T. Peraro, *Analytic multi-loop results using finite fields and dataflow graphs with FiniteFlow*, in *14th International Symposium on Radiative Corrections: Application of Quantum Field Theory to Phenomenology*, 12, 2019. [arXiv:1912.03142](#).
- [56] S. Abreu, J. Dormans, F. Febres Cordero, H. Ita, M. Kraus, B. Page, E. Pascual, M. Ruf, and V. Sotnikov, *Caravel: A c++ framework for the computation of multi-loop amplitudes with numerical unitarity*, *Computer Physics Communications* **267** (Oct., 2021) 108069.
- [57] F. V. Tkachov, *A Theorem on Analytical Calculability of Four Loop Renormalization Group Functions*, *Phys. Lett.* **100B** (1981) 65–68.
- [58] K. G. Chetyrkin and F. V. Tkachov, *Integration by Parts: The Algorithm to Calculate beta Functions in 4 Loops*, *Nucl. Phys. B* **192** (1981) 159–204.
- [59] S. Laporta, *High precision calculation of multiloop Feynman integrals by difference equations*, *Int. J. Mod. Phys. A* **15** (2000) 5087–5159, [[hep-ph/0102033](#)].
- [60] A. von Manteuffel and R. M. Schabinger, *A novel approach to integration by parts reduction*, *Phys. Lett. B* **744** (2015) 101–104, [[arXiv:1406.4513](#)].
- [61] T. Peraro, *Scattering amplitudes over finite fields and multivariate functional reconstruction*, *JHEP* **12** (2016) 030, [[arXiv:1608.01902](#)].
- [62] K. J. Larsen and Y. Zhang, *Integration-by-parts reductions from unitarity cuts and algebraic geometry*, *Phys. Rev. D* **93** (2016), no. 4 041701, [[arXiv:1511.01071](#)].
- [63] Z. Wu, J. Boehm, R. Ma, H. Xu, and Y. Zhang, *NeatIBP 1.0, a package generating small-size integration-by-parts relations for Feynman integrals*, *Comput. Phys. Commun.* **295** (2024) 108999, [[arXiv:2305.08783](#)].
- [64] X. Liu and Y.-Q. Ma, *Determining arbitrary Feynman integrals by vacuum integrals*, *Phys. Rev. D* **99** (2019), no. 7 071501, [[arXiv:1801.10523](#)].
- [65] X. Guan, X. Liu, Y.-Q. Ma, and W.-H. Wu, *Blade: A package for block-triangular form improved Feynman integrals decomposition*, *Comput. Phys. Commun.* **310** (2025) 109538, [[arXiv:2405.14621](#)].
- [66] T. Binoth, J. P. Guillet, and G. Heinrich, *Reduction formalism for dimensionally regulated one loop N point integrals*, *Nucl. Phys. B* **572** (2000) 361–386, [[hep-ph/9911342](#)].
- [67] G. Heinrich, *Sector Decomposition*, *Int. J. Mod. Phys. A* **23** (2008) 1457–1486, [[arXiv:0803.4177](#)].
- [68] G. Heinrich, S. P. Jones, M. Kerner, V. Magerya, A. Olsson, and J. Schlenk, *Numerical scattering amplitudes with pySecDec*, *Comput. Phys. Commun.* **295** (2024) 108956, [[arXiv:2305.19768](#)].
- [69] G. Barucchi and G. Ponzano, *Differential equations for one-loop generalized Feynman integrals*, *J. Math. Phys.* **14** (1973) 396–401.
- [70] A. V. Kotikov, *Differential equations method: New technique for massive Feynman diagrams calculation*, *Phys. Lett. B* **254** (1991) 158–164.

- [71] A. V. Kotikov, *Differential equations method: The Calculation of vertex type Feynman diagrams*, *Phys. Lett. B* **259** (1991) 314–322.
- [72] T. Gehrmann and E. Remiddi, *Differential equations for two loop four point functions*, *Nucl. Phys. B* **580** (2000) 485–518, [[hep-ph/9912329](#)].
- [73] J. M. Henn, *Multiloop integrals in dimensional regularization made simple*, *Phys. Rev. Lett.* **110** (2013) 251601, [[arXiv:1304.1806](#)].
- [74] F. Moriello, *Generalised power series expansions for the elliptic planar families of Higgs + jet production at two loops*, *JHEP* **01** (2020) 150, [[arXiv:1907.13234](#)].
- [75] X. Liu, Y.-Q. Ma, and C.-Y. Wang, *A Systematic and Efficient Method to Compute Multi-loop Master Integrals*, *Phys. Lett. B* **779** (2018) 353–357, [[arXiv:1711.09572](#)].
- [76] X. Liu and Y.-Q. Ma, *AMFlow: A Mathematica package for Feynman integrals computation via auxiliary mass flow*, *Comput. Phys. Commun.* **283** (2023) 108565, [[arXiv:2201.11669](#)].
- [77] R.-J. Huang, D.-S. Jian, Y.-Q. Ma, D.-M. Mu, and W.-H. Wu, *Efficient computation of one-loop Feynman integrals and fixed-branch integrals to high orders in ε* , *Phys. Rev. D* **111** (2025), no. 9 094028, [[arXiv:2412.21054](#)].
- [78] L.-H. Huang, R.-J. Huang, and Y.-Q. Ma, *Tame multi-leg Feynman integrals beyond one loop*, [[arXiv:2412.21053](#)].
- [79] G. Ossola, C. G. Papadopoulos, and R. Pittau, *Reducing full one-loop amplitudes to scalar integrals at the integrand level*, *Nucl. Phys. B* **763** (2007) 147–169, [[hep-ph/0609007](#)].
- [80] G. Ossola, C. G. Papadopoulos, and R. Pittau, *CutTools: A Program implementing the OPP reduction method to compute one-loop amplitudes*, *JHEP* **03** (2008) 042, [[arXiv:0711.3596](#)].
- [81] R. K. Ellis, W. T. Giele, and Z. Kunszt, *A Numerical Unitarity Formalism for Evaluating One-Loop Amplitudes*, *JHEP* **03** (2008) 003, [[arXiv:0708.2398](#)].
- [82] R. K. Ellis, W. T. Giele, Z. Kunszt, and K. Melnikov, *Masses, fermions and generalized D-dimensional unitarity*, *Nucl. Phys. B* **822** (2009) 270–282, [[arXiv:0806.3467](#)].
- [83] C. F. Berger, Z. Bern, L. J. Dixon, F. Febres Cordero, D. Forde, H. Ita, D. A. Kosower, and D. Maitre, *An Automated Implementation of On-Shell Methods for One-Loop Amplitudes*, *Phys. Rev. D* **78** (2008) 036003, [[arXiv:0803.4180](#)].
- [84] A. van Hameren, C. G. Papadopoulos, and R. Pittau, *Automated one-loop calculations: A Proof of concept*, *JHEP* **09** (2009) 106, [[arXiv:0903.4665](#)].
- [85] A. van Hameren, *Multi-gluon one-loop amplitudes using tensor integrals*, *JHEP* **07** (2009) 088, [[arXiv:0905.1005](#)].
- [86] P. Mastrolia, G. Ossola, T. Reiter, and F. Tramontano, *Scattering AMplitudes from Unitarity-based Reduction Algorithm at the Integrand-level*, *JHEP* **08** (2010) 080, [[arXiv:1006.0710](#)].
- [87] S. Badger, B. Biedermann, and P. Uwer, *NGluon: A Package to Calculate One-loop Multi-gluon Amplitudes*, *Comput. Phys. Commun.* **182** (2011) 1674–1692, [[arXiv:1011.2900](#)].
- [88] G. Bevilacqua, M. Czakon, M. V. Garzelli, A. van Hameren, A. Kardos, C. G. Papadopoulos, R. Pittau, and M. Worek, *HELAC-NLO*, *Comput. Phys. Commun.* **184** (2013) 986–997, [[arXiv:1110.1499](#)].

- [89] T. Peraro, *Ninja: Automated Integrand Reduction via Laurent Expansion for One-Loop Amplitudes*, *Comput. Phys. Commun.* **185** (2014) 2771–2797, [[arXiv:1403.1229](#)].
- [90] J. Alwall, R. Frederix, S. Frixione, V. Hirschi, F. Maltoni, O. Mattelaer, H. S. Shao, T. Stelzer, P. Torrielli, and M. Zaro, *The automated computation of tree-level and next-to-leading order differential cross sections, and their matching to parton shower simulations*, *JHEP* **07** (2014) 079, [[arXiv:1405.0301](#)].
- [91] **GoSam** Collaboration, G. Cullen et al., *GOSAM-2.0: a tool for automated one-loop calculations within the Standard Model and beyond*, *Eur. Phys. J. C* **74** (2014), no. 8 3001, [[arXiv:1404.7096](#)].
- [92] F. Buccioni, J.-N. Lang, J. M. Lindert, P. Maierhöfer, S. Pozzorini, H. Zhang, and M. F. Zoller, *OpenLoops 2*, *Eur. Phys. J. C* **79** (2019), no. 10 866, [[arXiv:1907.13071](#)].
- [93] G. Bevilacqua, D. Canko, C. G. Papadopoulos, and A. Spourdalakis, *Two-loop amplitude computation with HELAC*, *PoS LL2024* (2024) 051.
- [94] V. Sotnikov, *Scattering amplitudes with the multi-loop numerical unitarity method*. PhD thesis, Freiburg U., Freiburg U., 9, 2019.
- [95] G. Ossola, C. G. Papadopoulos, and R. Pittau, *On the Rational Terms of the one-loop amplitudes*, *JHEP* **05** (2008) 004, [[arXiv:0802.1876](#)].
- [96] S. D. Badger, *Direct Extraction Of One Loop Rational Terms*, *JHEP* **01** (2009) 049, [[arXiv:0806.4600](#)].
- [97] S. Pozzorini, H. Zhang, and M. F. Zoller, *Rational Terms of UV Origin at Two Loops*, *JHEP* **05** (2020) 077, [[arXiv:2001.11388](#)].
- [98] J.-N. Lang, S. Pozzorini, H. Zhang, and M. F. Zoller, *Two-Loop Rational Terms in Yang-Mills Theories*, *JHEP* **10** (2020) 016, [[arXiv:2007.03713](#)].
- [99] J.-N. Lang, S. Pozzorini, H. Zhang, and M. F. Zoller, *Two-loop rational terms for spontaneously broken theories*, *JHEP* **01** (2022) 105, [[arXiv:2107.10288](#)].
- [100] G. Guennebaud, B. Jacob, et al., “Eigen v3.” <http://eigen.tuxfamily.org>, 2010.
- [101] E. Anderson, Z. Bai, C. Bischof, S. Blackford, J. Demmel, J. Dongarra, J. Du Croz, A. Greenbaum, S. Hammarling, A. McKenney, and D. Sorensen, *LAPACK Users’ Guide*. Society for Industrial and Applied Mathematics, Philadelphia, PA, third ed., 1999.
- [102] V. Shtabovenko, R. Mertig, and F. Orellana, *FeynCalc 10: Do multiloop integrals dream of computer codes?*, *Comput. Phys. Commun.* **306** (2025) 109357, [[arXiv:2312.14089](#)].
- [103] B. Ruijl, T. Ueda, and J. Vermaseren, *FORM version 4.2*, [[arXiv:1707.06453](#)].
- [104] S. Abreu, P. F. Monni, B. Page, and J. Usovitsch, *Planar Six-Point Feynman Integrals for Four-Dimensional Gauge Theories*, [[arXiv:2412.19884](#)].
- [105] G. Bevilacqua, D. Canko, C. G. Papadopoulos, and A. Spourdalakis, *Numerical evaluation of dimensionally regulated amplitudes*, work in progress.
- [106] C. G. Papadopoulos, D. Tommasini, and C. Wever, *The Pentabox Master Integrals with the Simplified Differential Equations approach*, *JHEP* **04** (2016) 078, [[arXiv:1511.09404](#)].
- [107] T. Gehrmann, J. M. Henn, and N. A. Lo Presti, *Pentagon functions for massless planar scattering amplitudes*, *JHEP* **10** (2018) 103, [[arXiv:1807.09812](#)].

- [108] D. Chicherin, T. Gehrmann, J. M. Henn, N. A. Lo Presti, V. Mitev, and P. Wasser, *Analytic result for the nonplanar hexa-box integrals*, *JHEP* **03** (2019) 042, [[arXiv:1809.06240](#)].
- [109] D. Chicherin, T. Gehrmann, J. M. Henn, P. Wasser, Y. Zhang, and S. Zoia, *All Master Integrals for Three-Jet Production at Next-to-Next-to-Leading Order*, *Phys. Rev. Lett.* **123** (2019), no. 4 041603, [[arXiv:1812.11160](#)].
- [110] S. Abreu, H. Ita, F. Moriello, B. Page, W. Tschernow, and M. Zeng, *Two-Loop Integrals for Planar Five-Point One-Mass Processes*, *JHEP* **11** (2020) 117, [[arXiv:2005.04195](#)].
- [111] D. D. Canko, C. G. Papadopoulos, and N. Syrrakos, *Analytic representation of all planar two-loop five-point Master Integrals with one off-shell leg*, *JHEP* **01** (2021) 199, [[arXiv:2009.13917](#)].
- [112] D. Chicherin and V. Sotnikov, *Pentagon Functions for Scattering of Five Massless Particles*, *JHEP* **20** (2020) 167, [[arXiv:2009.07803](#)].
- [113] S. Abreu, H. Ita, B. Page, and W. Tschernow, *Two-loop hexa-box integrals for non-planar five-point one-mass processes*, *JHEP* **03** (2022) 182, [[arXiv:2107.14180](#)].
- [114] D. Chicherin, V. Sotnikov, and S. Zoia, *Pentagon functions for one-mass planar scattering amplitudes*, *JHEP* **01** (2022) 096, [[arXiv:2110.10111](#)].
- [115] A. Kardos, C. G. Papadopoulos, A. V. Smirnov, N. Syrrakos, and C. Wever, *Two-loop non-planar hexa-box integrals with one massive leg*, *JHEP* **05** (2022) 033, [[arXiv:2201.07509](#)].
- [116] S. Badger, M. Becchetti, E. Chaubey, and R. Marzucca, *Two-loop master integrals for a planar topology contributing to $pp \rightarrow t\bar{t}j$* , *JHEP* **01** (2023) 156, [[arXiv:2210.17477](#)].
- [117] F. Febres Cordero, G. Figueiredo, M. Kraus, B. Page, and L. Reina, *Two-loop master integrals for leading-color $pp \rightarrow t\bar{t}H$ amplitudes with a light-quark loop*, *JHEP* **07** (2024) 084, [[arXiv:2312.08131](#)].
- [118] S. Abreu, D. Chicherin, H. Ita, B. Page, V. Sotnikov, W. Tschernow, and S. Zoia, *All Two-Loop Feynman Integrals for Five-Point One-Mass Scattering*, *Phys. Rev. Lett.* **132** (2024), no. 14 141601, [[arXiv:2306.15431](#)].
- [119] S. Abreu, D. Chicherin, V. Sotnikov, and S. Zoia, *Two-loop five-point two-mass planar integrals and double Lagrangian insertions in a Wilson loop*, *JHEP* **10** (2024) 167, [[arXiv:2408.05201](#)].
- [120] S. Badger, M. Becchetti, N. Giraudo, and S. Zoia, *Two-loop integrals for $t\bar{t} + \text{jet}$ production at hadron colliders in the leading colour approximation*, *JHEP* **07** (2024) 073, [[arXiv:2404.12325](#)].
- [121] J. Henn, A. Matijašić, J. Miczajka, T. Peraro, Y. Xu, and Y. Zhang, *Complete function space for planar two-loop six-particle scattering amplitudes*, [arXiv:2501.01847](#).
- [122] M. Becchetti, D. Canko, V. Chestnov, T. Peraro, M. Pozzoli, and S. Zoia, *Two-loop Feynman integrals for leading colour $t\bar{t}W$ production at hadron colliders*, [arXiv:2504.13011](#).
- [123] P. Bargiela and T.-Z. Yang, *On the finite basis of two-loop ‘t Hooft-Veltman Feynman integrals*, [arXiv:2503.16299](#).
- [124] G. Bevilacqua, D. Canko, C. G. Papadopoulos, and A. Spourdalakis, *Automated two-loop calculations: a proof of concept*, work in progress.